MOLECULAR AND CELLULAR BIOLOGY, June 1997, p. 3081–3093 Vol. 17, No. 6
0270-7306/97/$04.00+0

Structure-Function Analysis of *TAF130*: Identification and Characterization of a High-Affinity TATA-Binding Protein Interaction Domain in the N Terminus of Yeast $TAF_{II}130$

YU BAI, GINA M. PEREZ, JOSEPH M. BEECHEM, AND P. ANTHONY WEIL*

Department of Molecular Physiology and Biophysics, Vanderbilt University School of Medicine, Nashville, Tennessee 37232-0615

Received 2 January 1997/Returned for modification 26 February 1997/Accepted 18 March 1997

We report structure-function analyses of *TAF130*, the single-copy essential yeast gene encoding the 130,000-M_r yeast TATA-binding protein (TBP)-associated factor $TAF_{II}130$ ($yTAF_{II}130$). A systematic family of *TAF130* mutants was generated, and these mutant *TAF130* alleles were introduced into yeast in both single and multiple copies to test for their ability to complement a *taf130*Δ null allele and support cell growth. All mutant proteins were stably expressed in vivo. The complementation tests indicated that a large portion (amino acids 208 to 303 as well as amino acids 367 to 1037) of $yTAF_{II}130$ is required to support cell growth. Direct protein blotting and coimmunoprecipitation analyses showed that two N-terminal deletions which remove portions of $yTAF_{II}130$ amino acids 2 to 115 dramatically decrease the ability of these mutant $yTAF_{II}130$ proteins to bind TBP. Cells bearing either of these two *TAF130* mutant alleles also exhibit a slow-growth phenotype. Consistent with these observations, overexpression of TBP can correct this growth deficiency as well as increase the amount of TBP interacting with $yTAF_{II}130$ in vivo. Our results provide the first combined genetic and biochemical evidence that $yTAF_{II}130$ binds to yeast TBP in vivo through $yTAF_{II}130$ N-terminal sequences and that this binding is physiologically significant. By using fluorescence anisotropy spectroscopic binding measurements, the affinity of the interaction of TBP for the N-terminal TBP-binding domain of $yTAF_{II}130$ was measured, and the K_d was found to be about 1 nM. Moreover, we found that the N-terminal domain of $yTAF_{II}130$ actively dissociated TBP from TATA box-containing DNA.

TFIID, one of the multiple eukaryotic general transcription factors (GTFs), plays a key role in DNA-dependent RNA polymerase II (RNAP II)-mediated transcription initiation and regulation. The form and function of TFIID have been extensively studied by using in vitro approaches (see references 7, 22, and 57 for recent reviews). TFIID exists as a stable multisubunit complex in a variety of distinct eukaryotic systems (7, 17, 22, 47, 57, 92), and in vitro transcription assays have shown that one subunit of TFIID, the TATA-binding protein (TBP), is sufficient for TATA element DNA recognition and subsequent incorporation of the other GTFs and RNAP II into the preinitiation complex (PIC). A TBP-assembled PIC can catalyze basal transcription in vitro (6, 67). However, these same in vitro assays also demonstrate that activation of transcription by sequence-specific DNA binding transactivator proteins can be observed only from a PIC formed by utilizing the multisubunit TBP-containing complex, TFIID, and not with TBP (32, 64). This observation suggested that the other subunits of TFIID are essential for its regulatory functions and ultimately led to the identification of the TBP-associated factors (TAFs), which in combination with TBP comprise the TFIID complex (17, 47, 64, 92).

At least 8 to 10 RNAP II-specific TAFs (or TAF_{II}s) associate with TBP to form eukaryotic TFIID. These TAF_{II}s exhibit molecular masses ranging from 250 to 15 kDa, depending on the organism analyzed (human, *Drosophila melanogaster*, and *Saccharomyces cerevisiae*) (17, 47, 61, 66, 92; see reference 7 for a recent review). A comparison of the amino acid sequences of TAF_{II}s from these evolutionarily divergent organisms shows that there is a striking conservation of TAF_{II} sequences (7). The results of various biochemical analyses have led to the hypothesis that TAF_{II}s participate in a variety of protein-protein and protein-DNA interactions. These interactions range from the facilitation of the formation and/or stabilization of the PIC by TAF_{II} binding to DNA (78, 82, 83) to TAF_{II}s interacting with each other (7, 29, 30, 33, 34, 37, 41–46, 53, 71, 79, 80, 83, 86, 87, 89, 91) or with basal transcription factors (7, 23, 26, 30, 42, 90) to the direct interaction of TAF_{II}s with the activation domains of transcriptional regulatory molecules (9, 11, 12, 19–21, 23, 31, 37, 42, 51, 72, 75, 80, 81, 86). Clearly, TAF_{II}s are involved in a large number of critical regulatory events in RNAP II transcription, and detailed analyses of TAF_{II} molecules will shed light on the molecular mechanisms of RNAP II transcriptional regulation.

The largest subunit of metazoan TFIID has been termed either $hTAF_{II}250$ or $dTAF_{II}250$, depending on whether it is a human or *Drosophila* protein. The human protein, $hTAF_{II}250$, contains an acidic N terminus, a central region including a high-mobility-group (HMG) homology box, and two bromodomain-like direct repeats, as well as a glycine- and serine-rich C terminus (29, 71). The *Drosophila* homolog, $dTAF_{II}250$, has >90% similarity and >50% identity at the amino acid level with its human counterpart (45, 86). Although the yeast homolog of $h/dTAF_{II}250$, $yTAF_{II}130$, is only half the size of the metazoan proteins, this yeast TAF_{II} still bears significant sequence similarity to the two metazoan proteins (61, 66; detailed in this report).

Using various in vitro techniques, the potential functions of metazoan $TAF_{II}250$ have begun to be elucidated. First, $hTAF_{II}250$ appears to link cell cycle regulation to transcrip-

* Corresponding author. Mailing address: Department of Molecular Physiology and Biophysics, Vanderbilt University School of Medicine, 746 Medical Research Building I, Nashville, TN 37232-0615. Phone: (615) 322-7007 or (615) 322-7008. Fax: (615) 322-7236. E-mail: tony.weil@mcmail.vanderbilt.edu.

tion. This conclusion is based on the fact that hTAF$_{II}$250 is encoded by *CCG1*, a gene which when mutant confers a temperature-sensitive G_1 growth arrest to a hamster cell line termed ts13 at elevated temperatures (29, 71, 73, 74). ts13 cells carry a mutation in *CCG1*. Detailed molecular analyses indicate that the mutant allele of *CCG1* in ts13 cells contains a point mutation at TAF$_{II}$250 amino acid 690 (25). Moreover, Wang and Tjian (85) found that either addition of purified human TFIID to nuclear transcription extracts prepared from ts13 cells or transfection of the cDNA encoding wild-type (WT) hTAF$_{II}$250 into ts13 cells can rescue transcriptional activation defects of ts13 cells and cell extracts. A second proposed function of TAF$_{II}$250, that of a coactivator, is based on the observation that hTAF$_{II}$250 has been shown to interact with several distinct transcriptional regulatory proteins (9, 20, 75). Third, in vivo and in vitro experiments indicate that TAF$_{II}$250 interacts with a variety of other TAF$_{II}$s (43, 83, 86, 87, 89), indicating that perhaps in addition to playing a potential coactivator function in transactivation, h/dTAF$_{II}$250 can also play an important structural role as a kind of scaffold for the formation of the TFIID complex. Fourth, dTAF$_{II}$250 interacts with the RAP74 subunit of TFIIF, suggesting that dTAF$_{II}$250 may actively contribute to PIC assembly (70). Fifth, dTAF$_{II}$250 has been shown to contain two distinct types of catalytic activities, a histone acetyltransferase (HAT) function (54) and two discrete protein kinase domains which can either autophosphorylate dTAF$_{II}$250 or transphosphorylate TFIIF (14). Finally and perhaps most importantly, h/dTAF$_{II}$250 interacts with TBP directly (29, 45, 71, 79, 86, 91).

Given the pivotal, multifunctional role(s) of yTAF$_{II}$130 and its metazoan homologs, detailed analyses of this protein are clearly mandated. However, there are many controversies and inconsistencies between the results of the various investigators who work on TAF$_{II}$250. For example, using in vitro-generated mutant forms of TAF$_{II}$250, one group found that dTAF$_{II}$250 has two TBP-binding sites and that dTAF$_{II}$250 binding to TBP can inhibit the binding of TBP to TATA DNA (45, 48). In contrast, others have published that deletion of N-terminal sequences from dTAF$_{II}$250 has no effect on either TBP binding to dTAF$_{II}$250 or formation of a triple TBP-dTAF$_{II}$250-dTAF$_{II}$110 complex capable of mediating SP1 transcriptional activation in vitro (86). The general drawbacks of these studies of TAF$_{II}$250 structure and function are that the majority of the work was carried out solely by using in vitro systems and with qualitative rather than quantitative measurements of the binding interactions under study. Thus, performing complementary in vivo studies of TAF$_{II}$ function along with thermodynamically rigorous analyses of the relevant protein-protein and protein-DNA interaction becomes critical if we are to truly understand TFIID.

We report here the results of our in vitro and in vivo structure-function studies of *TAF130*, the yeast gene encoding yTAF$_{II}$130. Our analyses indicate that a large number of deletions of *TAF130* sequences which remove the regions of the protein that are highly conserved between yeast yTAF$_{II}$130 and its metazoan counterparts diminish or abolish its ability to support cell growth. Interestingly, deletion of yTAF$_{II}$130 N-terminal sequences induces a slow-growth phenotype. Our biochemical experiments indicate that yTAF$_{II}$130 N-terminal sequences directly interact with TBP, and consistent with this result, overexpression of TBP can rescue the slow-growth phenotype induced by deletion of yTAF$_{II}$130 N-terminal sequences. Detailed spectrosopic measurements of the interaction of TBP with a fragment of yTAF$_{II}$130 comprising N-terminal amino acids 1 to 100 corroborated these results and further indicated that the affinity of this interaction is quite high, in the nanomolar range. The implications of these findings regarding yTAF$_{II}$130 and TFIID function are discussed.

MATERIALS AND METHODS

Yeast strains, growth conditions, and yeast transformation. *S. cerevisiae* YPH252 (76), (*MAT*α *ura3-52 lys2-801^{amber} ade2-101^{ochre} trp1-Δ1 his3-Δ200 leu2-Δ1*) was used as the parental strain for the majority of the experiments described in this report. Plasmids were transformed into yeast by using the lithium acetate technique (36). YPH252 and its derivatives were propagated in either yeast extract-peptone medium supplemented with 0.004% (wt/vol) adenine and 2% (wt/vol) dextrose (YPAD) or yeast synthetic complete (SC) medium supplemented with variable nutrients as indicated by a one-letter code (H, L, T, and U, for histidine, leucine, tryptophan, and uracil, respectively) as detailed in the figure legends. Use of galactose as a carbon source is indicated by Gal, while the use of dextrose is not specified. Both sugars were used at a final concentration of 2% (wt/vol) (40). When appropriate, 5-fluoroorotic acid (5-FOA) was added to SC agar plates at a final concentration of 0.2% (wt/vol) (5). SC agar plates inoculated with yeast cells were incubated at the temperatures indicated in the figure legends. Photographs of the plates were taken at 24-h intervals to monitor growth.

S. cerevisiae YPH500 (76) (*MAT*α *ura3-52 lys2-801^{amber} ade2-101^{ochre} trp1-Δ63 his3-Δ200 leu2-Δ1*) was used in some experiments to make protein extract which served as a negative control. A partially purified yTFIID fraction was made from the protease-deficient *S. cerevisiae* strain BJ5457 (39), (*MAT*α *ura3-52 lys2-801 trp1 leu2-Δ1 his3-Δ200 pep4::HIS3 prb1-Δ1.6R can1 GAL*) as well as from a *TAF130* shuffled *S. cerevisiae* strain, YBY402′ (2) (*MAT***a** *ura3-52 LYS2 ADE2 trp1-Δ901 his3-Δ200 leu2-3,112 suc2-Δ9 Δtaf130::TRP1* pRS313-HA$_3$-TAF130-WT), as described previously (63). The yTFIID (Bio-Rex) fractions were used as positive controls in both far-Western protein blotting and immunoblotting analyses.

Construction of plasmids expressing *TAF130*. A 5,397-bp *Xma*I-to-*Xba*I *TAF130*-containing DNA fragment derived from a YEp24 (8) genomic *TAF130* clone was subcloned into *Xba*I/*Xma*I-digested pRS316 (76). This fragment contains ~0.9 kb of 5′- and ~1.3 kb of 3′-flanking *TAF130* DNA sequences. The resulting plasmid, termed pRS316-TAF130, served as the starting plasmid for the construction of all other *TAF130* expression plasmids. These additional plasmids either introduced various deletion mutations and/or tags (HA$_3$ [three copies of the influenza virus hemagglutinin {HA} epitope {YPYDVPDYA}], which is recognized by the commercially available monoclonal antibody [MAb] 12CA5 [88]) into *TAF130* sequences or moved *TAF130* sequences into plasmids with various prototrophic markers or different promoters. Details of the construction and/or sequences of these plasmids are available on request. All plasmids were sequenced to ensure the integrity of appropriate added and/or manipulated DNA sequences.

***TAF130* gene knockout yeast strain.** A *TAF130* knockout strain was constructed via the one-step gene disruption technique (69) by replacing the entire *TAF130* open reading frame (ORF) in YPH252 with *TRP1* sequences as detailed previously (61). The resulting haploid disruptant strain, covered by pRS316-TAF130, was termed YBY805.

Plasmid shuffle and cell viability assays. All yeast *TAF130* mutants, carried on the *HIS3*-marked yeast expression plasmid pRS313, were transformed into YBY805. These pseudodiploid strains were either directly used for various analyses or subjected to plasmid shuffle using 5-FOA to generate haploid yeast strains carrying only the *HIS3*-marked plasmid-borne *TAF130* allele.

Immunoblot analyses. Pseudodiploid yeast strains containing both WT untagged pRS316-TAF130 covering plasmid and either pRS313 vector or HA$_3$-tagged *TAF130* (WT or Δ1 to Δ17; see Fig. 2) carried on pRS313 (see above) were grown in supplemented SC medium at 30°C and harvested when cell densities reached an optical density at 600 nm (OD$_{600}$) of 2.5/ml. Ten OD$_{600}$ units of cells (~2×10^9 cells) from each strain was collected by centrifugation and frozen at −70°C. At this point, cells could be stored frozen for extended periods of time if desired. Cell were then rapidly thawed and lysed by rapid vortex mixing (six bursts of 60 s each, with 2 min of cooling between bursts) with 0.3 g of acid-washed glass beads in 200 μl of radioimmunoprecipitation assay buffer (150 mM NaCl, 50 mM Tris-HCl [pH 7.9], 2 mM EDTA, 2 mM EGTA, 1% Nonidet P-40, 0.5% deoxycholate, 0.1% sodium dodecyl sulfate [SDS], 1 mM dithiothreitol, 5 mM phenylmethylsulfonyl fluoride, 5 mM benzamidine, 10 μg of leupeptin per ml) as described previously (24). The protein concentration of each lysate supernatant was measured by the bicinchoninic acid method (Pierce). Total extract protein yields were constant between strains (±10%). A 200-μg portion of protein extract from each strain was fractionated via SDS-polyacrylamide gel electrophoresis (PAGE), using a 7.5% polyacrylamide gel, and tank electrotransferred in CAPS [3-(cyclohexylamino)-1-propanesulfonic acid] buffer (10 mM CAPS [pH 11.0], 10% methanol, 0.5 g of dithiothreitol per liter) to polyvinylidene (PVDF) membranes (Millipore) (61). HA$_3$-tagged proteins were detected with MAb 12CA5 (Boehringer Mannheim) and enhanced chemiluminescence (ECL). An aliquot of yeast TFIID fraction, purified through the Bio-Rex 70 (Bio-Rad) chromatography step from an HA$_3$-yTAF$_{II}$130-expressing yeast strain, was used as a positive control (63).

Far-Western protein-blotting analysis. TBP purification, labeling, and yTAF$_{II}$130 protein blotting with ^{32}P-labeled TBP were performed as described

previously (4, 35). HA_3-tagged WT- and Δ1 to Δ17 $yTAF_{II}130$ proteins were generated by using coupled transcription-translation (TNT system; Promega) from these ORFs subcloned into pSP72. Protein production in this system was monitored by using both immunoblotting (MAb 12CA5) and autoradiography of [^{35}S]methionine-labeled proteins following SDS-PAGE fractionation.

Co-IP of TBP and $yTAF_{II}130$. Pseudodiploid yeast strains expressing both WT untagged $yTAF_{II}130$ and HA_3-tagged WT or Δ1 to Δ17 mutant forms of $yTAF_{II}130$ were grown in supplemented SC medium. Cells were harvested upon reaching an OD_{600} of 2.5/ml. Approximately 10 OD_{600} units (~2×10^9 cells) of cells was lysed from each strain and resuspended with 2 ml of cold extraction buffer BA/150 [BA/150 consists of 20 mM HEPES-KOH (pH 7.6)–2 mM EDTA–2 mM EGTA–0.25% Nonidet P-40 containing 150 mM potassium acetate (pH 7.5), 5 mM dithiothreitol, 5 mM phenylmethylsulfonyl fluoride, 5 mM benzamidine, 10 μg of leupeptin per ml, 10 μg of aprotinin per ml, 2 μg of pepstatin A per ml, 100 μg of L-1-chlor-3-(4-tosylamido)-4-phenyl-2-butanon (TPCK) per ml, and one protease inhibitor cocktail tablet (Boehringer Mannheim) in 25 ml of BA/150] and equally divided into four 1.5-ml Eppendorf tubes, to each of which was added 1 g of chilled acid-washed glass beads. Following lysis by rapid vortex mixing (see above), soluble proteins were recovered by centrifugation (5 min, 15,000 × *g*). The glass beads were washed once with fresh BA/150 (0.5 ml per tube), and the supernatant of the wash solution was pooled together with the four lysates, which were all pooled (total volume of 4 ml). This 4-ml lysate was then distributed equally (1 ml) into four 1.5-ml Eppendorf tubes. Then 20 μl of a 1:1 protein A-Sepharose bead (Sigma)–BA/150 slurry was added to each tube, and this mixture was incubated at 4°C on a tiltboard for 15 min to absorb out proteins which nonspecifically interact with protein A-Sepharose. Protein A-Sepharose-bound proteins were removed by centrifugation, and this preclearing procedure was performed once more. One milliliter of the precleared lysate was then incubated for 1.5 h at 4°C on a tiltboard with either 2.5 μg of MAb 12CA5 cross-linked to protein A-Sepharose beads or 0.5 μg of immunoaffinity-purified anti-TBP immunoglobulin G (IgG). In the case of the anti-TBP IgG, immune complexes were recovered following a 30-min incubation with the addition of 5 μl of 1:1 protein A-Sepharose bead–BA/150 slurry. The other two 1-ml aliquots of precleared lysate were also incubated with 5 μl of 1:1 protein A-Sepharose bead–BA/150 slurry to serve as negative controls for coimmunoprecipitation (co-IP). Antibody-antigen complexes bound to beads were recovered by centrifugation and washed by centrifugation five times with 1 ml of BA/150. The immunoprecipitates (IPs) were then resuspended in 50 μl of 2× SDS sample buffer (1% [wt/vol] SDS, 0.6 M Tris-PO_4 [pH 8.8], 1 mM EDTA, 0.6 M β-mercaptoethanol, 10% [vol/vol] glycerol, 0.01% [wt/vol] bromophenol blue) and immediately frozen on dry ice until fractionated via SDS-PAGE. Proteins were denatured by heating for 5 min at 100°C, and the MAb 12CA5 IPs were loaded on an SDS–13.5% polyacrylamide gel for immunoblot detection of TBP by using anti-TBP polyclonal IgG, while the anti-TBP IgG immunoprecipitates were loaded on a an SDS–9% polyacrylamide gel for immunoblot detection of HA_3-tagged $yTAF_{II}130$ by using MAb 12CA5. Antigen-bound IgG on the blots was detected by using ECL.

Overexpression of TBP in yeast. The yeast TBP ORF, as a *Sal*I/*Bam*HI fragment (generated previously [62]), was subcloned into the following *Sal*I/*Bam*HI-digested vectors. (i) Plasmid $pTBP_p$, which was derived from pRS315 (76), contains 1,118 bp of TBP gene 5′-flanking and 403 bp of TBP gene 3′-flanking sequences, such that the resulting TBP expression construct, termed $pTBP_p$-TBP, is driven by TBP's own promoter (62). (ii) Plasmid pRS415-PGK_p was derived from pRS415 (Stratagene) into which was cloned the yeast *PGK* promoter and *PGK* terminator sequences (see reference 62 for details). In pRS415-PGK_p-TBP, expression of the TBP ORF is driven by the *PGK* promoter. (iii) Plasmid pRS425-PGK_p is pRS425 (Stratagene) plus the *PGK* promoter and terminator as in pRS415-PGK_p. In pRS425-PGK_p-TBP, the TBP ORF is driven by the *PGK* promoter but in this case on a multicopy 2μm plasmid (13).

Overexpression of $yTAF_{II}130N_{100}$ in yeast. The DNA sequences encoding the first 100 N-terminal amino acids of $yTAF_{II}130$ ($yTAF_{II}130N_{100}$) (to which *Xho*I ends had been introduced via site-directed mutagenesis) were subcloned into the *Xho*I site of the series of yeast expression vectors generated by Mumberg et al. (56) and designated pRS4*X*5-GAL*Y* (*X* = 1 for CEN/ARS or 2 for 2μm; *Y* = S for small UAS_{GAL} sequence, L for large UAS_{GAL} sequence, or 1 for entire UAS_{GAL}). A c-Myc tag (EQKLISEEDL) recognized by MAb 9E10 (18) and the simian virus 40 T-antigen nuclear localization signal (NLS) (TPPKKKRKV) (65) were introduced at the very N or C terminus of the *TAF130* ORF fragment by site-directed mutagenesis (49). Constructs are named pRS4*X*5-GAL*Y*-myc-$TAF130N_{100}$ for the genes without an NLS or pRS4*X*5-GAL*Y*-myc-$TAF130N_{100}$-NLS if the clones contained an NLS. These constructs, along with the appropriate vector controls, were transformed individually into YPH500 (76). To test the effect of overexpression of the N terminus of $yTAF_{II}130$ on growth, a series of dilutions (ranging from 0.06 to 0.001 OD_{600} unit) of these transformed cells was replica plated on SC plates and SC-Gal plates to induce overexpression of $yTAF_{II}130N_{100}$. These plates were incubated at 4, 12, 25, 30, 35, and 37°C, and photographs of plates were taken at 12- to 24-hour intervals to monitor the effects of overexpression of $yTAF_{II}130N_{100}$ on cell growth.

$yTAF_{II}130N_{100}$ expression levels were measured by SDS-PAGE and immunoblotting. Plasmid containing cells were grown in SC-Gal, while control strain YPH500 was grown in YPAGal, and cells were harvested upon reaching a density of ~1.5 OD_{600} units/ml. A 1.5 OD_{600} unit amount of cells from each strain was then lysed with 0.6 g of glass beads in 200 μl of radioimmunoprecipitation buffer, and 30 μg of the resulting protein extract was subjected to fractionation via SDS-PAGE (12% gel). The c-Myc-tagged proteins were detected by using MAb 9E10 and ECL.

Expression and purification of c-Myc-tagged $yTAF_{II}130N_{100}$ in *Escherichia coli*. The c-Myc-tagged $yTAF_{II}130N_{100}$ *Xho*I DNA fragment was also subcloned into *Xho*I-digested pRSET B (Invitrogen) to allow for overexpression and purification of this protein. The resulting $yTAF_{II}130N_{100}$ expression plasmid was termed pRSETB-myc-$TAF130N_{100}$. pRSETB-myc-$TAF130N_{100}$ was transformed into *E. coli* BL21(DE3)pLysE, and protein production was induced at an OD_{600} of ~0.5/ml by the addition of isopropyl-β-D-thiogalactopyranoside to 1 mM. The induced culture was incubated for 3 h at 37°C (77). This His_6–c-Myc-tagged $yTAF_{II}130N_{100}$ polypeptide was purified from cell lysates by using Ni-nitrilotriacetic acid affinity chromatography by elution from the affinity matrix with a 20 to 300 mM imidazole gradient (Qiagen). The extent of protein purification was monitored by SDS-PAGE. Protein purity, as estimated by SDS-PAGE analyses, was >95%. The resulting purified protein, at a known concentration, was used as a quantitative standard to estimate expression of c-Myc-tagged $yTAF_{II}130N_{100}$ protein in yeast via immunoblotting.

Expression and purification of TBP and $yTAF_{II}130$ for spectroscopic binding studies. A non-c-Myc-tagged variant of $yTAF_{II}130N_{100}$ was expressed and purified from *E. coli*. A DNA fragment encoding the first 100 amino acids of $yTAF_{II}130$ protein with *Xho*I ends (generated by site-directed mutagenesis) was subcloned into the *E. coli* expression vector pET-HIS at the *Xho*I site (10) to generate plasmid pET-HIS-$TAF130N_{100}$. The correct clone was transformed into *E. coli* BL21(DE3)pLysS. Expression and purification of the resulting protein were performed as described above for the c-Myc-tagged $yTAF_{II}130$ N-terminal fragment. In this case, two polypeptides representing proteins of 14 and 18 kDa were eluted from the Ni-nitrilotriacetic acid column by using a 20 to 300 mM imidazole gradient. These proteins were present at roughly a ratio of 1 to 4 (14 kDa:18 kDa). Immunoblotting experiments indicated that the 14-kDa peptide is a C-terminally digested degradation product of the full-length 18-kDa protein.

Yeast WT TBP was subcloned into pET-3a vector (68). Expression and purification of TBP were performed as described previously (35). Protein purity was estimated via SDS-PAGE to be >95%.

Spectroscopic analyses of the interaction of TBP with $yTAF_{II}130N_{100}$. Fluorescence anisotropy measurements were performed with a fluorophore-labeled synthetic oligonucleotide of 16 bp which contained a consensus TATA box (underlined) whose sequence was derived from the adenovirus major late promoter: 5′-GGCG<u>TATAAAA</u>TGCGG-3′.

The rhodamine-X isothiocyanate (R-491; Molecular Probes, Eugene, Oreg.) fluorophore was attached to the oligonucleotide via a 5′ amino linker (5′-Amino-Modifier C6; Glen Research, Sterling, Va.). The conditions of probe labeling, purification, and generation of duplex DNA were as described previously (60). Protein-DNA binding reaction mixtures contained 7% (wt/vol) glycerol, 100 mM NaCl, 7 mM $MgCl_2$, 20 mM HEPES-NaOH (pH 7.9), and 100 μg of bovine serum albumin (fraction V; Sigma) per ml. The fluorescently labeled DNA (4.8 nM) was preequilibrated with TBP (34 nM) for approximately 6 h. $yTAF_{II}130N_{100}$ was then added to the preequilibrated TBP-DNA solution at final concentrations of 8, 25, 35, 59, 87, 116, 173, 234, 345, and 882 nM.

Both time-resolved and steady-state anisotropy measurements were used to monitor the interaction of $yTAF_{II}130N_{100}$ with TBP. Pulsed laser excitation (4-MHz repetition rate, 1-ps pulse width, 580 nm) utilized an Nd:YAG (Coherent Antares, Santa Clara, Calif.) synchronously pumped Coherent 702 dye laser. The collimated fluorescence emission was passed through automated Glan Thompson polarizers (ISS Inc. Koala, Urbana, Ill.) and a SPEX (Edison, N.J.) 0.22-m emission monochromator (set at 620 nm) and focused onto a 6-μm Hamamatsu (Bridgewater, N.J.) microchannel plate detector (model R2809U). The polarizers were rotated between vertical and horizontal positions every 15 s. Time-correlated single-photon counting was performed as detailed previously (60). The data for the equilibrium binding titration were obtained as an average of 10 consecutive polarization measurements taken every 30 s. Full time-resolved anisotropy measurements of the binding endpoints were performed by using data sets with approximately 20,000 counts at the peak of the vertically polarized decay curve. The impulse response of the system was approximately 50-ps full-width half-maximum.

Competitive binding analysis was performed by simultaneous solution of the coupled binding equilibria:

$$\text{TBP-yTAF}_{II}130N_{100} \overset{a}{\rightleftharpoons} yTAF_{II}130N_{100} + \text{TBP} + \text{DNA} \overset{a}{\rightleftharpoons} \text{TBP-DNA}$$

$$K_{d_{(yTAF_{II}130N_{100})}} = \frac{[\text{TBP}]\,[yTAF_{II}130N_{100}]}{[\text{TBP} - yTAF_{II}130N_{100}]},\quad K_{d_{(TBP)}} = \frac{[\text{TBP}]\,[\text{DNA}]}{[\text{TBP} - \text{DNA}]}$$

At each $yTAF_{II}130N_{100}$ addition, the coupled binding equilibria were iteratively solved for an internally consistent set of concentrations, subject to the constraint that the free TBP concentration (which couples the two equations) must be identical. The previously determined (60) dissociation constant of 4 nM was used for the TBP-DNA interaction. The only unknown required to describe the competitive binding assay was therefore the intrinsic $yTAF_{II}130N_{100}$-TBP dissociation constant, and this was determined by using standard nonlinear data

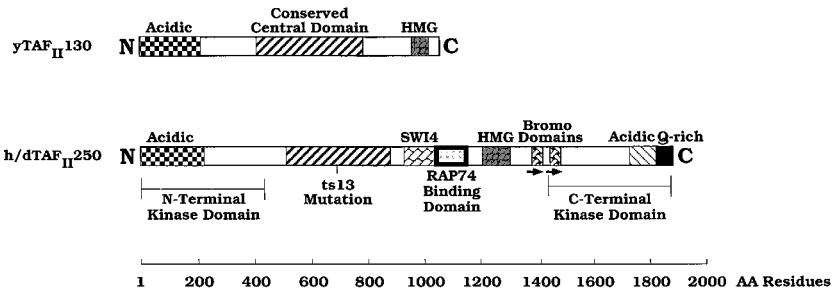

FIG. 1. Schematic representation of the alignment of yTAF$_{II}$130 with hTAF$_{II}$250 and dTAF$_{II}$250. The lower line indicates amino acid sequence positions. The three conserved regions between yTAF$_{II}$130 and h/dTAF$_{II}$250 referred to in the text are depicted N to C terminus as acidic, conserved central domain, and HMG. Several structural or functional motifs of h/dTAF$_{II}$250 noted by others (25, 29, 45, 70, 71, 86) are also indicated on the h/dTAF$_{II}$250 schematic (lower portion). The acidic domain refers to the 208-residue N-terminal region of yTAF$_{II}$130. This portion of yTAF$_{II}$130 exhibits a net negative charge of −31 and pI of 3.7 and resembles the 222-residue N-terminal portion of hTAF$_{II}$250, which exhibits a net negative charge of −32 and a calculated pI of 3.7. The corresponding region of dTAF$_{II}$250 (amino acids 1 to 230) has a net negative charge of −37 and calculated pI of 3.8. Overall, these regions have ~65% similarity. The conserved central domain of yTAF$_{II}$130 (overall ~60% similarity and 18% identity) comprises amino acid residues 440 to 830 of yTAF$_{II}$130, hTAF$_{II}$250 residues 560 to 968, and dTAF$_{II}$250 residues 607 to 1016. The putative yTAF$_{II}$130 HMG box extends from residues 937 to 1014 and is similar to the one in the C-terminal half of hTAF$_{II}$250 and dTAF$_{II}$250 (residues 1194 to 1275 and 1246 to 1362, respectively). Shown also in the sequence of TAF$_{II}$250 is the location of the hamster gene ts13 mutation in *CCG1* (25).

analysis techniques with rigorous error analysis (3). A single, uniquely defined chi-square minimum was observed when the raw anisotropy data were fitted to the yTAF$_{II}$130N$_{100}$-TBP dissociation constant.

RESULTS

Amino acid sequence conservation between yeast TAF$_{II}$130 and metazoan TAF$_{II}$250s. yTAF$_{II}$130, like metazoan TAF$_{II}$250, can interact directly with TBP in a protein-blotting assay (2, 29, 45, 66, 71, 79, 86, 91); therefore, functionally, at least by this criterion, TAF$_{II}$130 is the yeast homolog of h/dTAF$_{II}$250. Presumably, if these three proteins are true homologs, then elements of this TBP-binding region as well as other domains of these proteins should be conserved at the amino acid level. By using standard computer algorithms, the alignment of the amino acid sequences of yTAF$_{II}$130 with hTAF$_{II}$250 and dTAF$_{II}$250 shown in Fig. 1 was generated. Inspection of these alignments indicate that yTAF$_{II}$130 bears a striking sequence similarity to its metazoan counterparts in three distinct regions. First, yTAF$_{II}$130 N-terminal amino acids 1 to 208 are 65% similar to hTAF$_{II}$250 amino acids 1 to 222. These regions both have a calculated pI of 3.7 and exhibit nearly identical net negative charges, −31 for yTAF$_{II}$130 and −32 for the comparable region of hTAF$_{II}$250. The corresponding region of dTAF$_{II}$250 (amino acids 1 to 230) is also acidic in nature and has a net negative charge of −37 and calculated pI of 3.8. A second region of significant sequence similarity between these three TAF$_{II}$s is in the middle portion of these proteins, which comprises yTAF$_{II}$130 amino acids 440 to 830, hTAF$_{II}$250 amino acids 560 to 968, and dTAF$_{II}$250 amino acids 607 to 1016. In this portion of these TAF$_{II}$s, there is about 60% amino acid sequence similarity and 18% identity. Finally, like hTAF$_{II}$250 (29, 71) and dTAF$_{II}$250 (45), yTAF$_{II}$130 apparently contains an HMG homology box (2, 66). The sequences comprising the putative HMG homology box extend from yTAF$_{II}$130 amino acids 937 to 1014, while the corresponding regions in the metazoan TAF$_{II}$s are residues 1194 to 1275 for hTAF$_{II}$250 and amino acids 1246 to 1362 for dTAF$_{II}$250 (Fig. 1). The existence of these three highly conserved regions reinforces the concept that yTAF$_{II}$130 is the functional homolog of metazoan TAF$_{II}$250 and also implies that these conserved regions may play some key role(s) in yTAF$_{II}$130 function.

To test the functional significance of the observed sequence similarities of yTAF$_{II}$130 with h/dTAF$_{II}$250 and to begin to define the functional domains of yTAF$_{II}$130, we made a systematic family of deletion mutants of *TAF130* which spanned the entire *TAF130* ORF. The location and extent of each of these 17 deletions are depicted in Fig. 2. All deletion mutants were generated by site-directed mutagenesis of yTAF$_{II}$130 WT sequences, using single-stranded *TAF130* sequences as the template. Details of the mutagenesis protocol used are presented in Materials and Methods. The mutants are named yTAF$_{II}$130-Δ1 to -Δ17 in the order, from the N terminus to the

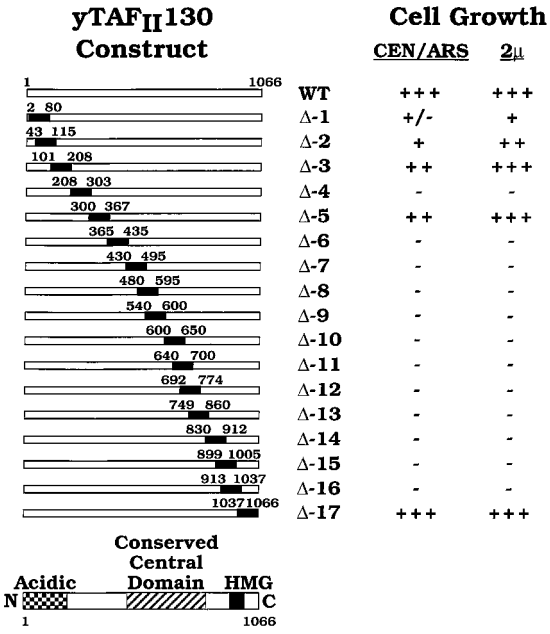

FIG. 2. Effects of deleting *TAF130* sequences on cell growth. The various deletion mutants of *TAF130* that were constructed are depicted at the left. The dark blocks and numbers refer to the amino acid residues deleted from yTAF$_{II}$130. The mutants are named Δ1 to Δ17, respectively, from N to C terminus as shown. A size-scaled schematic of yTAF$_{II}$130 with conserved sequence motifs labeled is shown at the bottom. The right panel shows the results of cell growth and viability tests conducted following 5-FOA plasmid shuffle performed as detailed in Materials and Methods. The WT and mutant *TAF130* genes expressing the indicated WT and mutant proteins were subcloned into both pRS313 (CEN/ARS) and pRS423 (2μm) plasmids as detailed in Materials and Methods. +, cell growth; −, no cell growth. The number of + signs indicates the relative growth rate of the cells. For both the CEN/ARS and 2μm families of plasmids, +++, ++, and + indicate visible colony growth in 4, 5, and 6 days, respectively, while +/− indicates visible growth in 10 to 14 days.

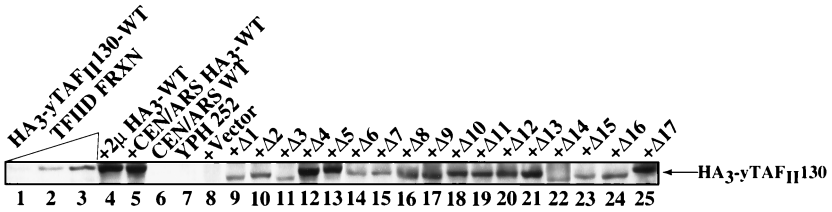

FIG. 3. Expression and stability of the various WT and mutant forms of $yTAF_{II}130$. A 200-μg portion of WCE protein extracted from the pseudodiploid strains expressing the indicated HA_3-tagged WT or mutant form of $yTAF_{II}130$ shown in Fig. 2 was electrophoresed on an SDS–7.5% polyacrylamide gel, electrotransferred to a PVDF membrane, and probed with MAb 12CA5 to detect HA_3-tagged $yTAF_{II}130$ proteins encoded by the pRS313-based *TAF130* genes. HA_3-tagged $yTAF_{II}130$ proteins were detected by ECL and are indicated by the arrow labeled HA_3-$yTAF_{II}130$ (lanes 5, and 9 to 25 for pRS313-HA_3-TAF130-WT and pRS313-HA_3-TAF130-Δ1 to -Δ17). Increasing amounts of an aliquot of partially purified yeast TFIID fraction (depicted by the triangle) derived from a HA_3-$yTAF_{II}130$ WT-expressing yeast strain were used as a positive control (labeled HA_3-$yTAF_{II}130$-WT TFIID FRXN). WCE proteins from the parental strain YPH252 or strains carrying pRS313 empty vector or untagged *TAF130-WT* served as negative controls (labeled as YPH 252, +Vector, or CEN/ARS WT, respectively). The HA_3-$yTAF_{II}130$-WT produced from pRS423 is shown in lane 4 and labeled +2μ HA_3-WT.

C terminus of $yTAF_{II}130$, in which they occur. This synoptic family of ca. 300-bp deletion mutants was used in both in vitro and in vivo systems to test the effect of removal of $yTAF_{II}130$ amino acid sequence on cell growth, TBP binding, and TFIID complex formation.

Deletion of $yTAF_{II}130$ N-terminal sequences induces a slow-growth phenotype. The *TAF130* deletion mutants *TAF130-Δ1* to *TAF130-Δ17* schematically depicted in Fig. 2 were subcloned into both single-copy CEN/ARS (pRS313) and multicopy 2μm (pRS423) yeast shuttle vectors. In all cases, *TAF130* expression is controlled by the normal *TAF130* 5′-flanking and 3′-flanking control elements. All of these constructs were separately transformed into YBY805, a yeast strain carrying a *taf130Δ::TRP1* null mutant allele in the chromosome and a *URA3*-marked pRS316-TAF130-WT covering plasmid. Interestingly, none of the resulting pRS313-TAF130 or pRS423-TAF130 constructs (WT or mutant) displayed a dominant negative phenotype, indicating that the presence of neither extra copies of the *TAF130* gene nor the tag sequences (HA_3) appended to *TAF130* had any apparent effect on cell growth (2) (see Fig. 7A). The ability of the various mutant *TAF130* alleles to complement growth of the *taf130Δ::TRP1* chromosomal null mutant gene was tested by plasmid shuffle using 5-FOA selection. The same number of cells from each *TAF130* pseudodiploid strain was inoculated by using a multiprong applicator onto multiple minimal medium plates either containing or lacking 5-FOA, and these plates were incubated at either 4, 12, 25, 30, 35, or 37°C to test for conditional complementation. The right portion of Fig. 2 summarizes the results of these cell viability complementation tests. As noted above, the tagged *TAF130-WT* allele can support cell growth as well as the untagged *TAF130* allele (2) regardless of whether the tagged gene was carried on a CEN/ARS or 2μm plasmid. When present on CEN/ARS plasmids, *TAF130* mutants Δ1, Δ2, Δ3, Δ5, and Δ17 grew, though only mutant Δ17 grew at the WT rate. Among the CEN/ARS constructs, $yTAF_{II}130$-Δ1 exhibited the slowest growth, followed by $yTAF_{II}130$-Δ2, while cells expressing only $yTAF_{II}130$-Δ3 and $yTAF_{II}130$-Δ5 grew just slightly slower than WT. To assess whether potential overexpression of these mutant *TAF130* alleles altered complementation patterns, the WT and mutant genes were expressed from a similar *HIS3*-marked plasmid, but in this case the plasmid carried 2μm replication and segregation sequences and thus should be present in multiple copies per cell (Fig. 2, far-right column). Among the 2μm constructs, $yTAF_{II}130$-Δ1 and -Δ2 did in fact grow slightly faster than their CEN/ARS counterparts, yet cells expressing these two forms of $yTAF_{II}130$ still grew slower than the rest of the other strains. Overexpression of mutants $yTAF_{II}130$-Δ3, and -Δ5 allowed these strains to grow at the same rate as $yTAF_{II}130$-WT. Finally, although the general complementation patterns were the same when tested at different temperatures, the slow-growth phenotypes of mutants Δ1, Δ2, Δ3, and Δ5 were exacerbated at 35 and 37°C. In aggregate, these results indicate that the N-terminal acidic region, the middle conserved central domain, and a portion of $yTAF_{II}130$ which resides near the C terminus, presumably the HMG homology region, all play important roles in normal $yTAF_{II}130$ function. Importantly, these essential regions are the three regions of high sequence conservation between $yTAF_{II}130$ and metazoan $TAF_{II}250$.

To analyze the expression of the various $yTAF_{II}130$ mutant proteins and to demonstrate that the observed patterns of noncomplementation were not simply caused by total protein instability, whole-cell extracts (WCEs) were prepared from all of the 36 pseudodiploid yeast strains shown in Fig. 2, and these cells were analyzed for $yTAF_{II}130$ content. As detailed in Materials and Methods, all of the $yTAF_{II}130$ proteins in these strains contain an HA_3 tag at their N termini; thus, immunoblotting of SDS-PAGE-fractionated WCE proteins with MAb 12CA5 will detect both the quantity and quality of HA_3-$yTAF_{II}130$ expressed in these strains. A 200-μg portion of protein lysate from each of these 36 yeast strains, along with various control proteins and extracts, was gel fractionated and electrotransferred to a PVDF membrane, HA_3-tagged proteins were detected by immunoblotting with MAb 12CA5, and antigen-antibody complexes were visualized by ECL detection. Shown in Fig. 3 are the results of this analysis, which was performed on yeast strains carrying the tagged WT allele and the 17 tagged mutant alleles of *TAF130* on the CEN/ARS plasmid pRS313. Comparable results were obtained (2) for the 18 cognate strains carrying these genes on the 2μm plasmid pRS423 (Fig. 3, lanes 4 and 5). In Fig. 3, a partially purified yTFIID fraction, prepared from yeast cells expressing HA_3-$yTAF_{II}130$ as the sole source of $yTAF_{II}130$, was used as a positive control. Increasing amounts of this TFIID fraction (HA_3-$yTAF_{II}130$-WT TFIID FRXN [Fig. 3, lanes 1 to 3]) served as a mobility and reactivity control. As expected, neither WT cells (YPH252 [Fig. 3, lane 7]) nor cells carrying empty vector pRS313 (Fig. 3, lane 8) or an untagged *TAF130* gene (CEN/ARS WT [Fig. 3, lane 6]) gave an immunoreactive signal, since no HA-tagged proteins should be present in these cells or WCEs. In contrast, overall, the complete set of pseudodiploid strains gave detectable HA_3-$yTAF_{II}130$ protein signals, indicating that all of the $yTAF_{II}130$ mutant proteins are stably expressed in these cells (i.e., mutants Δ1 to Δ17 [Fig. 3, lanes 9 to 25]), although there are differences in steady-state levels of $yTAF_{II}130$ in some of these mutants. In sum, we conclude that the lack of cell growth of cells expressing either *TAF130-Δ4* or

TAF130-Δ6 to *TAF130-Δ16* is not due to a simple lack of expression and/or total instability of the corresponding mutant yTAF$_{II}$130 proteins.

Deletion of yTAF$_{II}$130 N-terminal sequences dramatically reduces binding of TBP to yTAF$_{II}$130. To further dissect yTAF$_{II}$130 and to try to provide a molecular explanation for why some of the mutant alleles of *TAF130* could not complement our *taf130Δ::TRP1* null mutant, we examined the ability of each of the various forms of yTAF$_{II}$130 to directly bind TBP. A shared characteristic of yeast and metazoan yTAF$_{II}$130 homologs is that these proteins all directly bind TBP (2, 29, 45, 66, 71, 79, 86, 91). To monitor TBP-yTAF$_{II}$130 binding, we used a gel blotting technique whereby SDS-PAGE-fractionated and blotted yTAF$_{II}$130 was renatured and then incubated with ^{32}P-labeled TBP, and yTAF$_{II}$130-bound ^{32}P-TBP was detected by autoradiography. Control competition binding experiments (2) using unlabeled TBP and unlabeled chymotrypsinogen A (M_r = 25,000; pI = 9.4) and cytochrome *c* (M_r = 12,500; pI = 10.6) demonstrated that this far-Western protein-protein binding analysis specifically monitored yTAF$_{II}$130-TBP binding. Therefore, performing such analyses with our yTAF$_{II}$130 mutant protein collection should allow us to map the TBP-binding region(s) within yTAF$_{II}$130.

We used coupled transcription-reticulocyte lysate translation to generate the mutant and WT forms of yTAF$_{II}$130 for these analyses. To accomplish this, the WT and mutant *TAF130* ORFs were subcloned into the SP6 RNA polymerase promoter-driven plasmid pSP72 (see Materials and Methods for details). The resulting plasmids were used to program a coupled transcription-translation extract, and the in vitro-translated yTAF$_{II}$130 proteins generated were checked qualitatively and quantitatively by both direct detection of SDS-PAGE-fractionated [^{35}S]methionine-labeled yTAF$_{II}$130 translation products and MAb 12CA5 immunoblot analysis (2). Presented in Fig. 4A is the autoradiogram of SDS-PAGE-fractionated [^{35}S]methionine-labeled WT and mutant HA$_3$-yTAF$_{II}$130 polypeptides. Neither DNA buffer (T.1E [Fig. 4A, lane 1]) nor empty expression vector (pSP72 [Fig. 4A, lane 2]) programmed the synthesis of protein in this system as expected, while the positive control DNA template containing the luciferase ORF generated an mRNA which programmed the synthesis of the appropriate 61,000-M_r protein product (Fig. 4A, lane 3). All of the full-length HA$_3$-yTAF$_{II}$130 proteins were generated in vitro (Fig. 4A, lanes 4 to 21) at essentially identical levels. The relative mobilities of the various yTAF$_{II}$130 polypeptides are consistent with the mobilities of the corresponding in vivo-expressed HA$_3$-yTAF$_{II}$130 proteins shown in Fig. 3. yTAF$_{II}$130-WT contains 26 methionines, the same number of methionine residues as luciferase. Therefore, by using this information and the known specific activity of the [^{35}S]methionine, we calculated that the amount of yTAF$_{II}$130 proteins produced in vitro was approximately 40 to 60 ng/25-μl reaction. Fully 50% of the yTAF$_{II}$130 translation products were full-length proteins, though the prematurely terminated N-terminal polypeptide fragments are not shown here. This experiment confirms that yTAF$_{II}$130 proteins can be efficiently generated in this in vitro system; thus, we were in a position to use this method to produce yTAF$_{II}$130 for far-Western TBP binding assays.

For this purpose, we performed a second set of these coupled transcription-translation reactions except that only unlabeled amino acids were used for translation. The protein products of these reactions were fractionated by SDS-PAGE, electrotransferred to a membrane, denatured and renatured, and incubated with a ^{32}P-TBP probe as detailed in Materials and Methods. This analysis used the same set of WT and mutant samples analyzed in Fig. 4A with the addition of a positive control for TBP binding, a partially purified TFIID fraction. As expected, the yTAF$_{II}$130 in the TFIID fraction bound TBP (Fig. 4B, lane 1), while neither the reactions programmed with T.1E, empty vector pSP72, or pSP72-luciferase generated a 130,000-M_r protein capable of binding ^{32}P-TBP (Fig. 4B, lanes 2 to 4). HA$_3$-yTAF$_{II}$130-WT and mutants yTAF$_{II}$130-Δ3 to yTAF$_{II}$130-Δ17 bound ^{32}P-TBP with roughly equal efficiency (Fig. 4B, lanes 5 and 8 to 22). The reduction of TBP binding to mutant yTAF$_{II}$130-Δ8 is artifactual (Fig. 4B, lane 13) and was not observed in three other replicates of this experiment (2). Thus, mutants Δ3 through Δ17 all appear to bind TBP about as avidly as WT yTAF$_{II}$130. However, yTAF$_{II}$130-Δ1 and yTAF$_{II}$130-Δ2 mutant proteins reproducibly (2) displayed a dramatically reduced but finite ability to bind TBP (Fig. 4B, lanes 6 and 7, and reference 2). We conclude from the results of this experiment that the N terminus of yTAF$_{II}$130 plays a key, and perhaps major, role in mediating the interaction of TBP and yTAF$_{II}$130, at least under these in vitro assay conditions. This result taken together with the fact that Δ1 and Δ2 mutants grow slowly is consistent with the hypothesis that TBP interacts, perhaps directly, with yTAF$_{II}$130 N-terminal residues. It is important to note though that other TAF$_{II}$s probably also contribute significantly to the binding and/or stabilization of TBP in the TFIID complex (7).

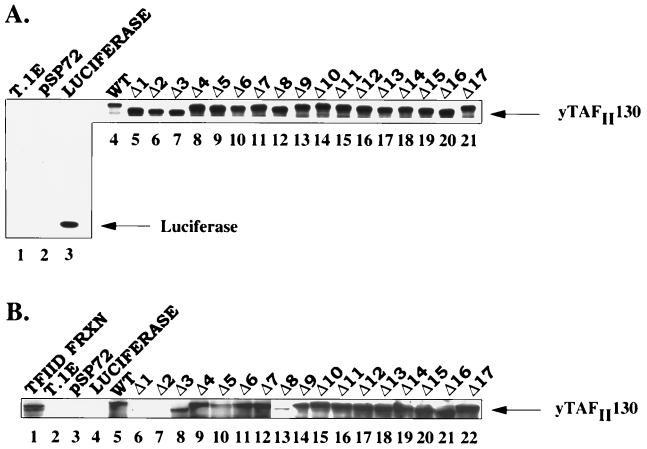

FIG. 4. Protein-protein binding assays map a high-affinity TBP interaction domain(s) to yTAF$_{II}$130 N-terminal amino acids 1 to 115. (A) Coupled transcription-translation reactions were carried out in the presence of [^{35}S]methionine as the labeling amino acid (22 μCi of [^{35}S]methionine/25-μl reaction; specific activity, 1,175 Ci/mmol). Twenty percent of each reaction (lanes 1 to 21) was fractionated via SDS-PAGE (9% gel); following electrophoresis, the gel was treated with an autoradiography enhancer (Entensify; NEN) and then dried and exposed to X-ray film. Only the portion of the autoradiogram displaying full-length yTAF$_{II}$130 translation products (indicated by the upper arrow) is shown. Scanning and quantitation of the complete autoradiogram indicated that >50% of all yTAF$_{II}$130 translation products were full length. (B) Unlabeled in vitro-translated yTAF$_{II}$130 protein products, as indicated (lanes 5 to 22), were fractionated via SDS-PAGE as described above and then electrotransferred to a nitrocellulose membrane, denatured and renatured, and probed with ^{32}P-labeled TBP (specific activity of TBP probe was about 6×10^6 cpm/μg; the concentration of probe in the binding reaction was about 13 nM). Following incubation with the TBP probe, the membrane was washed and exposed to X-ray film as detailed in Materials and Methods. Only the yTAF$_{II}$130 portion of the resulting autoradiogram is shown. ^{32}P-TBP bound to yTAF$_{II}$130 is indicated by the arrow and label. A partially purified yTFIID fraction (63) served as a positive control (lane 1, TFIID FRXN). Negative controls were as for panel A (lanes 2 to 4).

TBP interacts directly and with high affinity to yTAF$_{II}$130 N-terminal sequences. To unequivocably establish that TBP can interact directly with yTAF$_{II}$130 N-terminal sequences and, more importantly, to measure the affinity of this interaction, we used fluorescence-based spectroscopic analysis (16, 28,

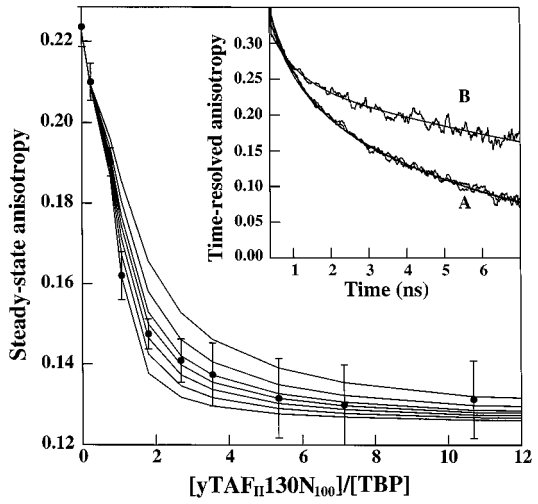

FIG. 5. Spectroscopic determination of the interaction of TBP and N-terminal yTAF$_{II}$130 sequences. Change in steady-state anisotropy of a preequilibrated sample of a fluorescently labeled DNA (5 nM)-TBP (35 nM) mixture with various quantities of yTAF$_{II}$130N$_{100}$ (8, 25, 35, 59, 87, 116, 173, 234, and 345 nM). The range of smooth lines through the data represents dissociation constants varying from (bottom to top) 0.5, 0.75, 1 (best-fit value), 1.25, 1.5, 2, and 3 nM. (Inset) Time-resolved anisotropies of fluorescently labeled TATA box DNA under the following conditions as discussed in the text. The three different experimental conditions which all produce an anisotropy pattern associated with completely unbound DNA are labeled A: reaction 1, 5 nM DNA alone; reaction 2, 5 nM DNA plus 500 nM yTAF$_{II}$130N$_{100}$; reaction 4, 5 nM DNA plus 35 nM TBP plus 500 nM yTAF$_{II}$130N$_{100}$. All three curves are shown superimposed. The curve labeled B represents the slower rotational dynamics in reaction 3, which contains DNA (5 nM) and TBP (35 nM) complexed.

38, 52, 60) to monitor TBP-yTAF$_{II}$130 interactions. These fluorescence anisotropy studies monitored the interaction of an N-terminal 100-amino-acid-long portion of yTAF$_{II}$130 identified by the experiments presented above as being important for both cell growth and TBP binding (Fig. 2 and 4). This fragment of yTAF$_{II}$130 was termed yTAF$_{II}$130N$_{100}$, and its interaction with TBP was measured by using a rhodamine-labeled TBP target TATA box oligonucleotide as a probe. Extensive equilibrium measurements of the interaction of yTAF$_{II}$130N$_{100}$ with TBP were made, and these experiments allowed us to show that yTAF$_{II}$130N$_{100}$ does indeed interact directly and with high affinity with TBP. A series of high-resolution time-resolved fluorescence anisotropy experiments was performed to initially characterize the number and nature of the DNA bound species associated with the titration of pre-bound TBP with yTAF$_{II}$130N$_{100}$. Figure 5 shows the results of time-resolved fluorescence anisotropy experiments performed at the following endpoint concentrations: reaction 1, free DNA (5 nM); reaction 2, DNA (5 nM) plus excess yTAF$_{II}$130N$_{100}$ (500 nM); reaction 3, DNA (5 nM) plus excess TBP (35 nM); and reaction 4, DNA (5 nM) plus excess TBP (35 nM) plus excess yTAF$_{II}$130N$_{100}$ (500 nM). We found that in reactions 1, 2, and 4, overlapping time-resolved fluorescence anisotropies were observed (overlapped curves, labeled A [Fig. 5, inset]). These three overlapping anisotropies corresponded to the intrinsic rotation of free DNA (rotational correlation time of approximately 7 ns). The intrinsic rotational rate of the TBP-bound TATA box DNA (reaction 3, labeled B [Fig. 5, inset]) was clearly resolved from the rotational behavior of the free DNA (correlation time of approximately 17 ns). These experiments revealed that excess yTAF$_{II}$130N$_{100}$ prevented TBP from interacting with TATA box-containing DNA. These experiments also revealed that yTAF$_{II}$130N$_{100}$ at these concentrations (500 nM) had no intrinsic affinity for the TATA box probe. Order-of-addition experiments (58) revealed that yTAF$_{II}$130N$_{100}$ not only prevented TBP from interacting with DNA but also actively dissociated pre-bound TBP from the DNA and that there were no fluorescence total-intensity lifetime changes in any of the samples measured. A full description of the stopped-flow kinetic versions of these experiments will be presented elsewhere (59).

Given these time-resolved fluorescence anisotropy results, a complete set of equilibrium competition experiments was performed (Fig. 5). We found that upon addition of increasing concentrations of yTAF$_{II}$130N$_{100}$ to preformed TBP-DNA complexes, full dissociation of TBP from DNA could be obtained. For each added increment of yTAF$_{II}$130N$_{100}$, a decrease in the observed steady-state anisotropy was observed. Since at these concentrations yTAF$_{II}$130N$_{100}$ has no affinity for the TATA box DNA, the observed steady-state anisotropy decrease must be the result of a direct interaction of yTAF$_{II}$130N$_{100}$ with TBP. This direct interaction decreases the free TBP concentration and hence by mass action "pulls" the TBP-DNA equilibrium toward the free DNA signal. Importantly, the observed binding titrations were completely reversible, indicating that yTAF$_{II}$130N$_{100}$ is not covalently modifying TBP to produce this result (58).

Full nonlinear analysis of the competition experiment was able to resolve a single high-affinity dissociation constant of 1 nM for the yTAF$_{II}$130N$_{100}$-TBP interaction (Fig. 5). Rigorous error analysis was performed to determine uncertainties on the recovered dissociation constant (3). The extreme ranges for the recovered dissociation constant were 0.75 nM $< K_d <$ 1.3 nM (at 67% confidence) and 0.4 nM $< K_d <$ 1.75 nM (at 95% confidence). These results demonstrate that the yTAF$_{II}$130N$_{100}$-TBP interaction is of even higher affinity, by approximately fourfold, than the specific binding constant of TBP for TATA box DNA, which is approximately 4 nM (60).

Co-IP assays using yeast WCEs also suggest that TBP interacts with yTAF$_{II}$130 N-terminal sequences. The results of the in vitro far-Western TBP-TAF binding experiments presented in Fig. 4 as well as of fluorescence spectroscopic analyses in Fig. 5 indicated that TBP interacts directly and specifically with yTAF$_{II}$130, particularly through this TAF's N-terminal sequences. We reasoned that if TBP really did interact more weakly with yTAF$_{II}$130 mutants Δ1 and Δ2, then in WCEs from these strains prepared under mild conditions, less of the yTAF$_{II}$130-TBP complex (i.e., TFIID) should be detectable by co-IP assay. Moreover, identical results should be obtained regardless of the precipitating antibody used, either anti-TBP IgG or anti-TAF antibody (here anti-HA MAb 12CA5). To test this hypothesis, we performed a series of experiments where the yTAF$_{II}$130-TBP complex content of WCE prepared from WT cells was compared with the amount of TBP-yTAF$_{II}$130 complex in WCEs prepared from control WT nontagged, Δ1, and Δ4 mutant *TAF130* strains. *TAF130-Δ4* here served as a control because despite the fact that yTAF$_{II}$130-Δ4 binds TBP well (Fig. 4B, lane 9), it does not complement the *taf130Δ::TRP1* null allele (Fig. 2). In this experiment, we analyzed strains carrying the various *TAF130* alleles on both CEN/ARS and 2μm plasmids, and the results are presented in Fig. 6. Prior to performance of the critical co-IP studies, several features of both the WCEs prepared from the yeast strains used for these experiments and our immunological procedures were established (2). First, we showed that all extracts contained the same amount of TBP. Second, we demonstrated that appropriate amounts of yTAF$_{II}$130 (i.e., WT, Δ1, and Δ4) proteins were present in all of the WCEs used. These analyses also showed that neither changes in *TAF130* expression (i.e.,

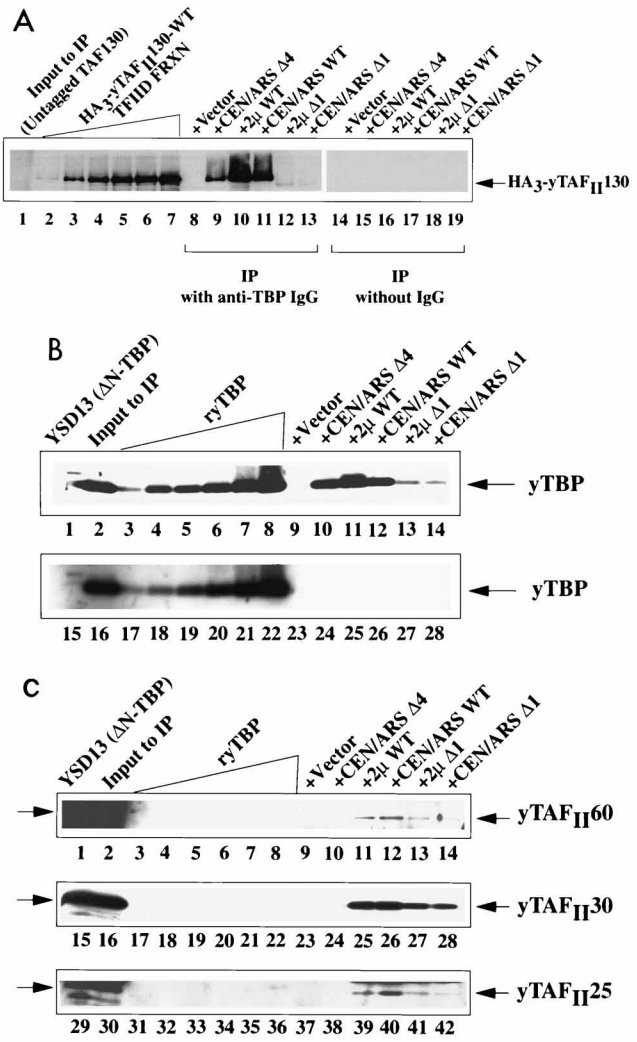

FIG. 6. Co-IP assays indicate that TBP interacts with yTAF$_{II}$130 N-terminal sequences. (A) Protein A-Sepharose-precleared WCE proteins were incubated with either 0.5 μg of immunoaffinity-purified anti-TBP IgG (lanes 8 to 13) or BA/150 buffer (lanes 14 to 19) as detailed in Materials and Methods. The IPs formed were harvested with protein A-Sepharose, fractionated via SDS-PAGE (9% gel), and immunoblotted with MAb 12CA5 to detect the HA$_3$-tagged yTAF$_{II}$130 proteins that were complexed with TBP. The specific HA$_3$-yTAF$_{II}$130 protein signal is indicated by the arrow and yTAF$_{II}$130 label. A partially purified yTFIID fraction (63) served as a positive control (lanes 2 to 7). (B) Protein A-Sepharose-precleared WCE proteins were incubated with either 2.5 μg of MAb 12CA5 protein A-Sepharose (lanes 9 to 14) or with protein A-Sepharose (lanes 23 to 28) as a negative precipitation control as detailed in Materials and Methods. The resulting immunoprecipitates were fractionated by SDS-PAGE (13.5% gel). TBP coimmunoprecipitating with yTAF$_{II}$130 (lanes 9 to 14) was detected by immunoblotting the SDS-PAGE-fractionated and electroblotted proteins with anti-TBP IgG. The TBP signals are shown by the arrows. The triangle indicates increasing amounts (0.25 to 8 ng) of purified recombinant yeast TBP (ryTBP) (35) that was used as a positive and quantitation control (lanes 3 to 8 and lanes 17 to 22). The co-IP input from the pseudodiploid strain containing the pRS313 vector was also used to show the existence of endogenous TBP in this strain (lanes 2 and 16). ΔN-TBP (62) served as a negative control (lanes 1 and 15). (C) The immunoblot filters used for the experiment shown in panel B were stripped and sequentially reprobed with anti-yTAF$_{II}$60, anti-yTAF$_{II}$30, and anti-yTAF$_{II}$25 polyclonal antibodies. TAF$_{II}$ antigen-antibody complexes were detected by ECL in every case. The arrows and labels indicate the positions of the corresponding yTAF$_{II}$s recognized by their antibodies (yTAF$_{II}$60, yTAF$_{II}$30, and yTAF$_{II}$25). The triangle shows the lanes where increasing amounts of purified recombinant yeast TBP had been loaded (lanes 3 to 8, 17 to 22, and 31 to 36; see panel B), while lanes 1 and 2, 15 and 16, and 29 and 30 were used as positive controls to show the position of endogenous yTAF$_{II}$60, yTAF$_{II}$30, and yTAF$_{II}$25, respectively. The ECL film exposure shown was for 1 min. This extended exposure was required to detect the yTAF$_{II}$60 signal in lanes 9 to 14. In a 1-s exposure, defined bands representing endogenous yTAF$_{II}$60 were observed in lanes 1 and 2 (2).

copy number) nor TBP expression levels significantly altered steady-state levels of the other protein (2). Third, we determined that all IP reactions were conducted under conditions of antibody excess. Finally, we showed that both HA$_3$-tagged and nontagged yTAF$_{II}$130 could be immunoprecipitated from solution with equal efficiency.

The results of our TBP-yTAF$_{II}$130 co-IP analyses are shown in Fig. 6A and B. In this experiment, IPs were formed with the proteins present in the various WCEs with either anti-TBP (Fig. 6A) or anti-HA MAb 12CA5 (Fig. 6B) to form immune complexes with TBP and associated proteins or yTAF$_{II}$130 and associated proteins. The resulting IPs were fractionated by SDS-PAGE, blotted, and probed for either the amount of yTAF$_{II}$130 coimmunoprecipitating with TBP (Fig. 6A, lanes 8 to 13) compared with no-IgG control IP reactions (Fig. 6A, lanes 14 to 19) or the amount of TBP coimmunoprecipitating with yTAF$_{II}$130 (Fig. 6B, lanes 9 to 14) compared with no-antibody control IP reactions (Fig. 6B, lanes 23 to 28). In both cases, the same quantitation and specificity controls were used (i.e., yeast HA$_3$-tagged TFIID fraction [63] and recombinant TBP or WCE from a strain expressing ΔN-TBP, which is not recognized by our polyclonal anti-TBP IgG [62]). All co-IP signals observed are specific since generation of either coimmunoprecipitated TBP or coimmunoprecipitated yTAF$_{II}$130 required addition of an HA$_3$ tag to *TAF130* (Fig. 6A, lanes 8 and 11; Fig. 6B, lanes 9 and 12) and addition of appropriate antibodies (Fig. 6A, lanes 14 to 19; Fig. 6B, lanes 23 to 28). Importantly, it is clear from these results that there is less of the yTAF$_{II}$130-TBP complex in WCE prepared from the yeast strain expressing yTAF$_{II}$130-Δ1 compared to either yTAF$_{II}$130-WT or yTAF$_{II}$130-Δ4, regardless of whether this mutant gene is carried on a CEN/ARS or 2μm plasmid (Fig. 6A [compare lanes 12 and 13 with lanes 9 to 11]; Fig. 6B [compare lanes 13 and 14 with lanes 10 to 12]). We conclude, on the basis of these results, that as predicted, there is less of the yTAF$_{II}$130-TBP complex in cells harboring the Δ1 mutant allele of *TAF130*.

To further examine if the decreased yTAF$_{II}$130-TBP complex content phenotype was a major deficiency of cells carrying the mutant *TAF130-Δ1* allele and to test if the residual yTAF$_{II}$130-TBP complex present in this strain could participate normally in TFIID assembly, an extension of the co-IP experiment shown in Fig. 6C was performed. We figured that if reduced TBP binding was the major defect of yTAF$_{II}$130-Δ1, then when the TFIID multisubunit TBP-TAF complex was immunoprecipitated with anti-TAF MAb 12CA5 IgG (from the HA$_3$-tagged *TAF130* strains), the normal complement of RNAP II-specific yTAF$_{II}$s (61, 66) should be coimmunoprecipitated. Moreover, the relative amount of coimmunoprecipitating TAF$_{II}$s should mirror the reduced amount of yTAF$_{II}$130-TBP complex observed in Fig. 6A and B. We thus took the membrane upon which the IPs of Fig. 6B were analyzed, stripped off the bound anti-TBP antibody, and sequentially reprobed the membrane with anti-yTAF$_{II}$60 IgG, anti-yTAF$_{II}$30 IgG, and finally anti-yTAF$_{II}$25 IgG. The results of these additional analyses are presented in Fig. 6C. As expected, none of the three yTAF$_{II}$s which we probed for were coimmunoprecipitated when there was no HA$_3$-yTAF$_{II}$130 in the extracts (Fig. 6C, lanes 9, 23, and 37). yTAF$_{II}$60, -30, and -25 did, however, coimmunoprecipitate efficiently with HA$_3$-yTAF$_{II}$130-WT from yeast strains carried on both CEN/ARS and 2μm plasmids (Fig. 6C, lanes 11, 12, 25, 26, 39, and 40). These same yTAF$_{II}$s also coimmunoprecipitated with HA$_3$-yTAF$_{II}$130-Δ1, though somewhat less efficiently than WT, as predicted. This reduction in TFIID content was evident whether *TAF130-Δ1* was carried on a CEN/ARS or 2μm plasmid (Fig. 6C, lanes 13, 14, 27, 28, 41, and 42). Interestingly, none of these three

yTAF$_{II}$s appear associated with HA$_3$-yTAF$_{II}$130-Δ4, as there is essentially no immunoreactive signal for any of these yTAF$_{II}$s on these blots (Fig. 6C; compare lanes 10, 24, and 38 with lanes 11 to 14, 25 to 28, and 39 to 42). This result with the yTAF$_{II}$130-Δ4 mutant protein was obtained despite the fact that yTAF$_{II}$130-Δ4 bound TBP as efficiently as the WT protein (Fig. 4B, lane 9; Fig. 6B, lane 10).

In aggregate, the results of the co-IP experiments presented in Fig. 6 strongly suggest that a major binding site for TBP resides within the N-terminal portion of yTAF$_{II}$130. Further, despite the fact that yTAF$_{II}$130-Δ1 and yTAF$_{II}$130-Δ2 exhibit reduced affinity for TBP, these mutant proteins can still productively interact with TBP and other yTAF$_{II}$s to form the TFIID complex. Mutant yTAF$_{II}$130-Δ4, however, is apparently totally deficient in TAF$_{II}$-TAF$_{II}$ interactions but not in interaction with TBP. Clearly, binding of yTAF$_{II}$130 to TBP is a necessary but not sufficient interaction for TFIID formation and function.

TBP overexpression both corrects the slow-growth phenotype of *TAF130*-Δ*1* and increases the intracellular content of yTAF$_{II}$130-TBP complex. The results of the experiments described above (Fig. 4 to 6) argue that TBP interacts specifically with yTAF$_{II}$130 sequences in the region of N-terminal amino acids 1 to 115. Further, in the strain carrying *TAF130*-Δ*1*, which exhibits slow growth, there is less TBP complexed with yTAF$_{II}$130. Thus, if the decreased amount of the TBP-yTAF$_{II}$130-TFIID complex was directly or indirectly responsible for this slow growth, we hypothesized that by increasing the amount of TBP complexed with yTAF$_{II}$130 through mass action by increasing the intracellular content of TBP, we should be able to correct the slow-growth phenotype of this strain. We directly tested this hypothesis as follows. We constructed three *LEU2*-marked TBP expression plasmids, two based on single-copy CEN/ARS plasmids (pRS315 and pRS415) and one based on a multicopy 2μm plasmid (pRS425). These plasmids utilized either the TBP or *PGK* promoter to drive TBP gene transcription. The resulting plasmids, either with (Fig. 7A, pRS315-TBP$_p$-TBP, pRS415-PGK$_p$-TBP, and pRS425-PGK$_p$-TBP) or without (pRS315-TBP$_p$, pRS415-PGK$_p$, and pRS425-PGK$_p$) the TBP ORF were then introduced into the four pseudodiploid yeast strains indicated in Fig. 7A as V (*taf130*Δ*::TRP1*, pRS316-TAF130-WT, pRS313), WT (*taf130*Δ*::TRP1*, pRS316-TAF130-WT, pRS313-HA$_3$-TAF130-WT), Δ1 C/A (*taf130*Δ*::TRP1*, pRS316-TAF130-WT, pRS313-HA$_3$-TAF130-Δ1), and Δ1 2μ (*taf130*Δ*::TRP1*, pRS316-TAF130-WT, pRS423-HA$_3$-TAF130-Δ1). These four isogenic *TAF130* pseudodiploid yeast strains differed only in the second *HIS3*-marked plasmid which they contained (V, vector pRS313; WT, pRS313-TAF130-WT; Δ1 C/A, pRS313-TAF130-Δ1; Δ1 2μ, pRS423-TAF130-Δ1). The resulting 24 yeast strains generated by transformation with the TBP expression plasmids and vectors were subjected to the plasmid shuffle assay to uncover the *HIS3*-marked plasmids. These yeast strains were inoculated, first onto appropriate SC plates containing 5-FOA and then onto SC plates lacking 5-FOA. Control experiments (2) directly demonstrated that introduction of the three TBP expression plasmids (Fig. 7A, top right) resulted in increases in TBP content. Moreover, these control experiments (2) also showed that TBP overexpression had no significant effect on total yTAF$_{II}$130 levels (WT or mutant). As expected (Fig. 2), cells carrying just pRS313 (Fig. 7A, plates labeled V, sectors 1 to 6) did not grow on 5-FOA whereas strains carrying pRS313-TAF130-Δ1 (Fig. 7A, plates labeled Δ1 C/A, sectors 1, 3, and 5) or pRS423-TAF130-Δ1 (Fig. 7A, plates labeled Δ1 2μ, sectors 1, 3, and 5) grew, albeit slowly, on 5-FOA-containing plates. Cells carrying *TAF130* on pRS313 grew well on 5-FOA, as would be expected (Fig. 7A, plates labeled WT, sectors 1 to 6). Importantly, overexpression of TBP in both strain Δ1 C/A (Fig. 7A, sectors 2, 4, and 6) and strain Δ1 2μ (Fig. 7A, sectors 2, 4, and 6) rescued the slow-growth phenotype of these yeast strains, which carried only the *TAF130*-Δ*1* mutant allele after 5-FOA shuffle. This result is entirely consistent with our working hypothesis, which posits that TBP interacts with the N-terminal sequences of yTAF$_{II}$130.

Co-IP assays were next performed with this set of six WCEs. IPs were formed by using the anti-HA-specific MAb 12CA5, which will recognize HA$_3$-tagged yTAF$_{II}$130-Δ1 protein and associated proteins in these extracts. The IPs were harvested and fractionated by SDS-PAGE, blotted, and probed for TBP content. If TBP overexpression caused an increase in yTAF$_{II}$130-TBP complex formation, there should be more coimmunoprecipitated TBP in the MAb 12CA5 IP. This is precisely the result obtained. As shown in Fig. 7B (compare lanes 2, 4, and 6 with lanes 1, 3, and 5), overexpression of TBP causes more TBP to coimmunoprecipitate with yTAF$_{II}$130-Δ1 protein, particularly when TBP is highly (10- to 20-fold [2]) overexpressed. This result is entirely consistent with our model that yTAF$_{II}$130 N-terminal sequences comprise a TBP interaction site(s).

In an attempt to provide further support for this idea, we generated a family of variously *UAS$_{GAL}$*-regulated plasmids which expressed an ORF encoding yTAF$_{II}$130N$_{100}$ (see Materials and Methods for details). Appended to this ORF were two additional elements, the sequences encoding the simian virus 40 T-antigen NLS (TPPKKKRKV) (65) and the c-Myc epitope tag (EQKLISEEDL) (18), which was used to quantitate and monitor expression. The rationale behind this experiment was that use of *UAS$_{GAL}$*-controlled expression vectors (56) would allow us to conditionally overexpress yTAF$_{II}$130N$_{100}$. If TBP interacts with yTAF$_{II}$130 through the N terminus of the TAF protein, then overexpressed polypeptide comprising this domain of yTAF$_{II}$130 should compete with the intact protein for TBP binding, resulting in a galactose-dependent cell slow-growth phenotype. We generated a family of *GAL-TAF$_{II}$130N$_{100}$* ORF plasmids, which were introduced into a variety of different haploid and diploid WT and mutant yeast strains (YPH250, -252, and -274, YPH499, -500, and -501 [76], SEY6210, -6211, and -6210.5 [27], and Δ1, Δ2, Δ3, Δ5, Δ17, and WT *TAF130* strains [Fig. 2]) to test this idea. Unfortunately, despite the fact that the yTAF$_{II}$130N$_{100}$ protein was stably expressed, no effects of its expression were noted (2). The reasons for this negative result are unknown; obviously a final resolution to this question will require further experimentation.

DISCUSSION

A variety of elegant in vitro biochemical studies of TAFs have shown that these molecules play an important role in RNAP II-mediated transcription (7, 22, 57). However, in order to ultimately apply these and other data to elucidate the detailed mechanisms underlying transcription and transcriptional regulation, the results of in vitro analyses must be complemented by both genetic and quantitative biochemical approaches (1, 15, 16, 55, 60, 84). Here, we report structure-function analyses of yeast *TAF130*, the single-copy essential gene encoding the 130,000-M_r subunit of yTFIID (61, 66), the homolog of metazoan TAF$_{II}$250, by taking advantage of the genetic and biochemical tractability of the *S. cerevisiae* system. Through the biochemical, biophysical, and genetic analyses reported here, we present the first detailed structure-function analysis of a eukaryotic TAF-encoding gene. We have also demonstrated that yTAF$_{II}$130 binds to TBP both in vivo and in vitro, primarily though not exclusively through yTAF$_{II}$130 N-

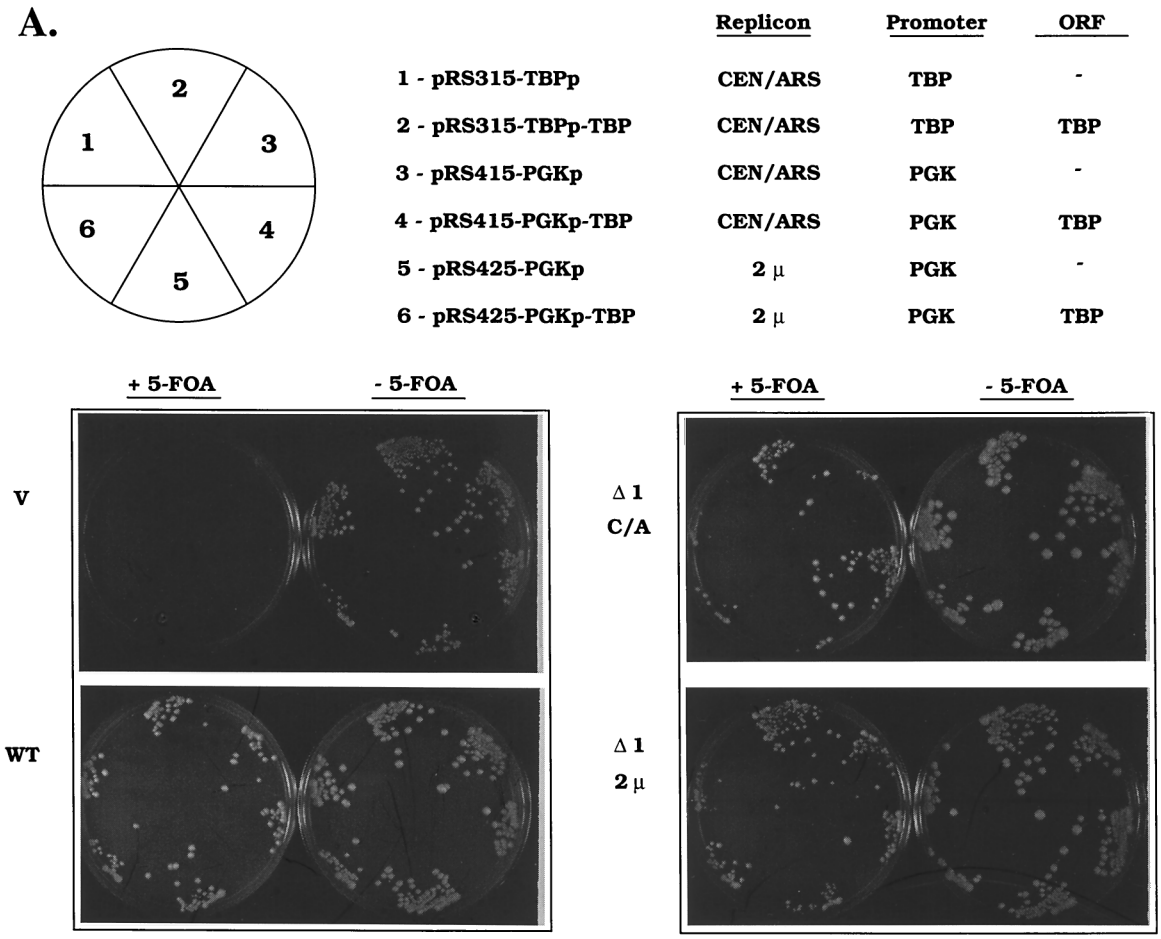

FIG. 7. Overexpression of TBP both corrects the slow-cell-growth phenotype of the yTAF$_{II}$130-Δ1-expressing strain and increases the amount of TBP binding to yTAF$_{II}$130-Δ1 protein. (A) The right side of the upper portion of panel A shows the important components of each TBP overexpression plasmid: 1, pRS315-TBP$_p$ (vector with TBP promoter but no TBP ORF); 2, pRS315-TBP$_p$-TBP (TBP promoter driving the TBP ORF); 3, pRS415-PGK$_p$ (vector with *PGK* promoter but no TBP ORF); 4, pRS415-PGK$_p$-TBP (*PGK* promoter driving the TBP ORF); 5, pRS425-PGK$_p$ (2μm plasmid vector with *PGK* promoter but no TBP ORF); 6, pRS425-PGK$_p$-TBP (*PGK* promoter driving the TBP ORF in the 2μm plasmid). The left side schematically indicates the position of each numbered strain located on the plates shown in the lower portion. The lower portion shows the growth of each strain carrying the indicated TBP construct streaked on the SC-supplemented plates in the presence (+) or absence (−) of 5-FOA. The pseudodiploid strains (*taf130Δ::TRP1*, pRS316-TAF130-WT) plated also contain either pRS313 vector (V), pRS313-HA$_3$-TAF130-WT (WT), pRS313-HA$_3$-TAF130-Δ1 (Δ1 C/A), or pRS423-HA$_3$-TAF130-Δ1 (Δ1 2μ). (B) Protein A-Sepharose-precleared WCE proteins from the yeast strains containing *TAF130-Δ1* and vectors or the various cognate TBP-expressing constructs detailed in panel A were incubated with 2.5 μg of MAb 12CA5 cross-linked to protein A-Sepharose beads. The IPs formed were subjected to an immunoblot analysis with anti-TBP IgG and ECL. The arrow indicates the position of TBP on the blot. The TBP construct contained in each strain is shown at the top.

terminal sequences. This result substantiates our own previous results (2) and the results of others (66). These data also support the work of Kokubo et al. (45, 48), who showed that TBP could interact with the N-terminal sequences of both intact dTAF$_{II}$250 and N-terminal fragments of this protein with roughly equal efficiencies. Interestingly, deletion of the N-terminal TBP-binding region from yTAF$_{II}$130 induces a slow-growth phenotype. This slow-growth phenotype can be suppressed by overexpression of TBP, suggesting that TBP interacts directly, specifically, and with high affinity with this domain of yTAF$_{II}$130. Using immunological and spectroscopic techniques, we confirmed that there is high affinity of interaction of TBP with the N-terminal portion of yTAF$_{II}$130 and that at least in vitro, this interaction is direct.

The effects of our family of deletion mutants of yTAF$_{II}$130 on cell viability showed not only that the very N terminus of yTAF$_{II}$130 is important for function but that two other regions of yTAF$_{II}$130 also play important roles in cell physiology. The integrity of both the conserved central domain and a small C-terminal portion of yTAF$_{II}$130 was also found to be critical for yTAF$_{II}$130 function(s). This finding is consistent with the fact that these three regions of yTAF$_{II}$130 are evolutionarily conserved between yeast and humans.

Our alignments of yTAF$_{II}$130 and HMG sequences show that the putative yTAF$_{II}$130-HMG homology region extends from amino acids 937 to 1014. This region of yTAF$_{II}$130 is deleted in yTAF$_{II}$130-Δ16. However, according to the align-

ments reported by others (29, 45, 66, 71, 86), the putative HMG homology region extends from yTAF$_{II}$130 amino acid 952 to very near the C terminus of the protein (i.e., amino acids 952 to 1049). If one considers the entire interval from yTAF$_{II}$130 amino acids 952 to 1049 to comprise the HMG homology region, then both yTAF$_{II}$130-Δ16 and -Δ17 have had a portion of this HMG homology region deleted. Our data suggest that amino acids 952 to 1037 perhaps are the most important sequences in this regard, since cells only expressing the *TAF130-Δ16* form of yTAF$_{II}$130 are inviable.

Deletion of yTAF$_{II}$130 N-terminal sequences induces a cell slow-growth phenotype relative to cells expressing WT yTAF$_{II}$130. This effect is more severe in cells expressing yTAF$_{II}$130-Δ1 than in cells expressing yTAF$_{II}$130-Δ2, suggesting that the first 50 amino acids of yTAF$_{II}$130 may play a more critical and/or dominant role in TBP binding. This conclusion is based on both our complementation and our co-IP experiments (2). If correct, this observation clearly demonstrates the power of the genetic complementation assays, since the far-Western TBP binding assays were not sensitive enough to pick up such potential differences in TBP binding affinity as apparently exist between the Δ1 and Δ2 forms of yTAF$_{II}$130. However, further detailed in vivo and in vitro binding assays must be performed to rigorously test the hypothesis that the N-terminal 50 amino acids of yTAF$_{II}$130 contribute the majority of the TBP binding energy of the N-terminal domain of this TAF. It will also be interesting to test if these viable mutant forms of yTAF$_{II}$130 (or -Δ3, -Δ5, and -Δ17) exhibit defects in cell cycle progression (73, 74). Preliminary microscopic examination of all *TAF130* deletion mutants placed on 5-FOA plates has failed to detect any obvious Cdc-like phenotypes for any of these mutants (2). Moreover, none of the viable *TAF130* mutants exhibit gross morphological changes (2).

The portion of yTAF$_{II}$130 sequence deleted in yTAF$_{II}$130 constructs Δ7 to Δ13 (i.e., conserved central domain) exhibits about 60% amino acid sequence similarity and 18% identity to the equivalent portion of the corresponding human and *Drosophila* TAF$_{II}$s. Since these mutants (Δ7 to Δ13) do not appear to affect the ability of yTAF$_{II}$130 to bind TBP, in the cell yTAF$_{II}$130 must display multiple functionalities. In vitro analyses of metazoan TAF$_{II}$250 performed by others reveal that these proteins make multiple protein-protein contacts with several different TAFs, such as hTAF$_{II}$135 (7), hTAF$_{II}$80 (30, 87), hTAF$_{II}$55 (12, 50), hTAF$_{II}$30 (37), dTAF$_{II}$150 (83), dTAF$_{II}$110 (43, 86), dTAF$_{II}$62 (87), and dTAF$_{II}$30β (89). Thus it is reasonable to envision that yTAF$_{II}$130 is also involved in making multiple TAF-TAF interactions and that this conserved central domain region may be responsible for these functionalities. As shown herein, one mutant allele, *TAF130-Δ4*, produces a form of yTAF$_{II}$130 that is apparently unable to interact efficiently with yTAF$_{II}$60, yTAF$_{II}$30, and yTAF$_{II}$25 even though this mutant protein can interact efficiently with TBP. However, additional preliminary co-IP analyses (2) indicate that there is little, if any, deficiency in TFIID assembly of mutant yTAF$_{II}$130 proteins Δ7 to Δ13 which have portions of the central conserved domain deleted. Although it is possible that mutant forms of yTAF$_{II}$130-Δ7 to -Δ13 interact less well with other TAF$_{II}$s, the in vitro conditions that we have used for our co-IP studies failed to accentuate this deficiency. Based on these considerations, we suggest that the C terminus of yTAF$_{II}$130, encompassed by deletions Δ7 to Δ13, may be involved in mediating interactions with other GTFs and/or transcriptional regulatory factors or yTAF$_{II}$130 endogenous enzymatic activities, such as to directly impact on the efficiency of RNAP II PIC formation and/or utilization. Indeed, it has recently been demonstrated that yTAF$_{II}$130 (and metazoan TAF$_{II}$250) has an endogenous HAT activity (54). This HAT activity was mapped to yTAF$_{II}$130 amino acid residues 354 to 817 (54), clearly within the central conserved domain. Additional experimentation will be required to test these hypotheses. Finally, the results obtained with *TAF130-Δ4* suggest that the interaction of TBP with yTAF$_{II}$130 is an early, if not the first, step of TFIID assembly, at least ahead of recruitment of yTAF$_{II}$60, -30, and -25 into the TFIID complex.

Although the combination of genetic complementation, co-IP, and far-Western analysis was capable of indicating the importance of direct yTAF$_{II}$130-TBP interactions, these methods are not easily used for the determination of thermodynamically rigorous binding affinities. However, fluorescence-based anisotropy spectroscopy is ideally suited for such determinations. Using this powerful method, one can perform binding studies at physiologically relevant concentrations (picomolar to nanomolar), and most importantly, no physical separation of the bound and free species is required. The detailed time-resolved and steady-state anisotropy measurements reported here clearly revealed that the presence of stoichiometric amounts of yTAF$_{II}$130N$_{100}$ can dissociate TBP from TATA box DNA. This result is consistent with the data of others who reported that dTAF$_{II}$250 N-terminal sequences appeared able to dissociate TBP from DNA (45, 48). Similar to what was found in our previous studies of protein-nucleic acid interactions (16, 60), there was no change in fluorescence lifetimes of any monitored species during any of the competitive binding isotherms that we have obtained (58). This result indicates that all of the fluorescence anisotropy change which is observed is associated with changes in the rotational properties of the bound DNA (i.e., dissociation). Rigorous nonlinear analysis of the competitive binding isotherms revealed a single, unique dissociation constant of 0.4 nM $< K_d <$ 1.75 nM for the yTAF$_{II}$130N$_{100}$-TBP interaction (at the 95% confidence level). A full study describing the kinetic mechanism association with this competitive inhibition of TBP binding TATA box DNA by yTAF$_{II}$130N$_{100}$ will be presented elsewhere (59). Interestingly, the largest uncertainty associated with the determination of the TBP-TAF dissociation constant is not actually related to the analysis of the raw (competition) anisotropy data but rather is related to how well the absolute protein concentrations of the TBP and yTAF$_{II}$130N$_{100}$ preparations can be determined. A combination of bicinchoninic acid protein assay, SDS-PAGE silver staining, and amino acid analyses was used here to determine TBP and yTAF$_{II}$130N$_{100}$ protein concentrations. However, an approximately twofold uncertainty in absolute protein concentrations remained with these analyses.

The data presented in this study represent a first but important step toward the characterization of the structure and function of yTAF$_{II}$130 and TFIID in an in vivo system. Though significant insights into the structure of this TFIID subunit have been obtained through the studies described in this report, much remains to be learned. Further quantitative biochemical and genetic studies of the effects of these and other (2) yTAF$_{II}$130 mutants on TAF-TAF and TAF-regulator interactions and TFIID assembly will clearly enhance our understanding of TFIID function in transcription regulation.

ACKNOWLEDGMENTS

We are grateful to Jeff Flick for Myc (9E10) MAb ascites and Todd Graham for yeast strains SEY6210 and 6211. We thank David Poon for his involvement in the early stages of this study and also members of our lab and department for freely sharing reagents, particularly Kevin Gerrish for the TAF preparation and George Patterson for the purified recombinant yeast TBP.

This research was supported by NIH grants GM52461 (P.A.W.) and RR5823 (J.M.B.).

REFERENCES

1. **Apone, L. M., C. A. Virbasius, J. C. Reese, and M. R. Green.** 1996. Yeast $TAF_{II}90$ is required for cell-cycle progression through G2/M but not for general transcription activation. Genes Dev. **10:**2368–2380.
2. **Bai, Y.** Unpublished observations.
3. **Beechem, J. M.** 1992. Global analysis of biochemical and biophysical data. Methods Enzymol. **210:**37–54.
4. **Blanar, M. A., and W. J. Rutter.** 1992. Interaction cloning: identification of a helix-loop-helix zipper protein that interacts with c-Fos. Science **256:**1014–1018.
5. **Boeke, J. D., J. Trueheart, G. Natsoulis, and G. R. Fink.** 1987. 5-Fluoroorotic acid as a selective agent in yeast molecular genetics. Methods Enzymol. **154:**164–175.
6. **Buratowski, S., S. Hahn, P. A. Sharp, and L. Guarente.** 1988. Function of a yeast TATA element-binding protein in a mammalian transcription system. Nature (London) **334:**37–42.
7. **Burley, S. K., and R. G. Roeder.** 1996. Biochemistry and structural biology of transcription factor IID (TFIID). Annu. Rev. Biochem. **65:**769–799.
8. **Carlson, M., and D. Botstein.** 1982. Two differentially regulated mRNAs with different 5′ ends encode secreted and intracellular forms of yeast invertase. Cell **28:**145–154.
9. **Carrozza, M. J., and N. A. DeLuca.** 1996. Interaction of the viral activator protein ICP4 with TFIID through TAF250. Mol. Cell. Biol. **16:**3085–3093.
10. **Chen, B. P., and T. Hai.** 1994. Expression vectors for affinity purification and radiolabeling of proteins using *Escherichia coli* as host. Gene **139:**73–75.
11. **Chen, J. L., L. D. Attardi, C. P. Verrijzer, K. Yokomori, and R. Tjian.** 1994. Assembly of recombinant TFIID reveals differential coactivator requirements for distinct transcriptional activators. Cell **79:**93–105.
12. **Chiang, C. M., and R. G. Roeder.** 1995. Cloning of an intrinsic human TFIID subunit that interacts with multiple transcriptional activators. Science **267:**531–536.
13. **Christianson, T. W., R. S. Sikorski, M. Dante, J. H. Shero, and P. Hieter.** 1992. Multifunctional yeast high-copy-number shuttle vectors. Gene **110:**119–122.
14. **Dikstein, R., S. Ruppert, and R. Tjian.** 1996. $TAF_{II}250$ is a bipartite protein kinase that phosphorylates the base transcription factor RAP74. Cell **84:**781–790.
15. **Dikstein, R., S. Zhou, and R. Tjian.** 1996. Human $TAF_{II}105$ is a cell type-specific TFIID subunit related to $hTAF_{II}130$. Cell **87:**137–146.
16. **Dunkak, K., M. R. Otto, and J. M. Beechem.** 1996. Real-time fluorescence assay system for gene transcription: simultaneous observation of protein/DNA binding, localized DNA melting, and mRNA production. Anal. Biochem. **243:**234–244.
17. **Dynlacht, B. D., T. Hoey, and R. Tjian.** 1991. Isolation of coactivators associated with the TATA-binding protein that mediate transcriptional activation. Cell **66:**563–576.
18. **Evan, G. I., G. K. Lewis, G. Ramsay, and J. M. Bishop.** 1985. Isolation of monoclonal antibodies specific for human c-*myc* proto-oncogene product. Mol. Cell. Biol. **5:**3610–3616.
19. **Ferreri, K., G. Gill, and M. Montminy.** 1994. The cAMP-regulated transcription factor CREB interacts with a component of the TFIID complex. Proc. Natl. Acad. Sci. USA **91:**1210–1213.
20. **Geisberg, J. V., J. L. Chen, and R. P. Ricciardi.** 1995. Subregions of the adenovirus E1A transactivation domain target multiple components of the TFIID complex. Mol. Cell. Biol. **15:**6283–6290.
21. **Gill, G., E. Pascal, Z. H. Tseng, and R. Tjian.** 1994. A glutamine-rich hydrophobic patch in transcription factor Sp1 contacts the $dTAF_{II}110$ component of the *Drosophila* TFIID complex and mediates transcriptional activation. Proc. Natl. Acad. Sci. USA **91:**192–196.
22. **Goodrich, J. A., G. Cutler, and R. Tjian.** 1996. Contacts in context: promoter specificity and macromolecular interactions in transcription. Cell **84:**825–830.
23. **Goodrich, J. A., T. Hoey, C. J. Thut, A. Admon, and R. Tjian.** 1993. *Drosophila* $TAF_{II}40$ interacts with both a VP16 activation domain and the basal transcription factor TFIIB. Cell **75:**519–530.
24. **Harlow, E., and D. Lane.** 1988. Antibodies a laboratory manual. Cold Spring Harbor Laboratory Press, Cold Spring Harbor, N.Y.
25. **Hayashida, T., T. Sekiguchi, E. Noguchi, H. Sunamoto, T. Ohba, and T. Nishimoto.** 1994. The *CCG1/TAF$_{II}$250* gene is mutated in thermosensitive G1 mutants of the BHK21 cell line derived from golden hamster. Gene **141:**267–270.
26. **Henry, N. L., A. M. Campbell, W. J. Feaver, D. Poon, P. A. Weil, and R. D. Kornberg.** 1994. TFIIF-TAF-RNA polymerase II connection. Genes Dev. **8:**2868–2878.
27. **Herman, P. K., and S. D. Emr.** 1990. Characterization of *VPS34*, a gene required for vacuolar protein sorting and vacuole segregation in *Saccharomyces cerevisiae*. Mol. Cell. Biol. **10:**6742–6754.
28. **Heyduk, T., Y.-X. Ma, H. Tang, and R. H. Ebright.** 1996. Fluorescence anisotropy: rapid, quantitative assay for protein-DNA and protein-protein interaction. Methods Enzymol. **274:**492–503.
29. **Hisatake, K., S. Hasegawa, R. Takada, Y. Nakatani, M. Horikoshi, and R. G. Roeder.** 1993. The p250 subunit of native TATA box-binding factor TFIID is the cell-cycle regulatory protein CCG1. Nature (London) **362:**179–181.
30. **Hisatake, K., T. Ohta, R. Takada, M. Guermah, M. Horikoshi, Y. Nakatani, and R. G. Roeder.** 1995. Evolutionary conservation of human TATA-binding-polypeptide-associated factors $TAF_{II}31$ and $TAF_{II}80$ and interactions of $TAF_{II}80$ with other TAFs and with general transcription factors. Proc. Natl. Acad. Sci. USA **92:**8195–8199.
31. **Hoey, T., R. O. Weinzierl, G. Gill, J. L. Chen, B. D. Dynlacht, and R. Tjian.** 1993. Molecular cloning and functional analysis of *Drosophila TAF110* reveal properties expected of coactivators. Cell **72:**247–260.
32. **Hoffmann, A., E. Sinn, T. Yamamoto, J. Wang, A. Roy, M. Horikoshi, and R. G. Roeder.** 1990. Highly conserved core domain and unique N terminus with presumptive regulatory motifs in a human TATA factor (TFIID). Nature (London) **346:**387–390.
33. **Hoffmann, A., C. M. Chiang, T. Oelgeschlager, X. Xie, S. K. Burley, Y. Nakatani, and R. G. Roeder.** 1996. A histone octamer-like structure within TFIID. Nature (London) **380:**356–359.
34. **Hoffmann, A., and R. G. Roeder.** 1996. Cloning and characterization of human *TAF20/15*. Multiple interactions suggest a central role in TFIID complex formation. J. Biol. Chem. **271:**18194–18202.
35. **Horikoshi, M., C. K. Wang, H. Fujii, J. A. Cromlish, P. A. Weil, and R. G. Roeder.** 1989. Cloning and structure of a yeast gene encoding a general transcription initiation factor TFIID that binds to the TATA box. Nature (London) **341:**299–303.
36. **Ito, H., Y. Fukuda, K. Murata, and A. Kimura.** 1983. Transformation of intact yeast cells treated with alkali cations. J. Bacteriol. **153:**163–168.
37. **Jacq, X., C. Brou, Y. Lutz, I. Davidson, P. Chambon, and L. Tora.** 1994. Human $TAF_{II}30$ is present in a distinct TFIID complex and is required for transcriptional activation by the estrogen receptor. Cell **79:**107–117.
38. **Jameson, D. M., and W. H. Sawyer.** 1995. Fluorescence anisotropy applied to biomolecular interactions. Methods Enzymol. **246:**283–300.
39. **Jones, E. W.** 1991. Tackling the protease problem in *Saccharomyces cerevisiae*. Methods Enzymol. **194:**428–453.
40. **Kaiser, C., S. Michaelis, and A. Mitchell.** 1994. Methods in yeast genetics: a Cold Spring Harbor Laboratory course manual. Cold Spring Harbor Laboratory Press, Cold Spring Harbor, N.Y.
41. **Klebanow, E. R., D. Poon, S. Zhou, and P. A. Weil.** 1996. Isolation and characterization of *TAF25*, an essential yeast gene that encodes an RNA polymerase II-specific TATA-binding protein-associated factor. J. Biol. Chem. **271:**13706–13715.
42. **Klemm, R. D., J. A. Goodrich, S. Zhou, and R. Tjian.** 1995. Molecular cloning and expression of the 32-kDa subunit of human TFIID reveals interactions with VP16 and TFIIB that mediate transcriptional activation. Proc. Natl. Acad. Sci. USA **92:**5788–5792.
43. **Kokubo, T., D. W. Gong, R. G. Roeder, M. Horikoshi, and Y. Nakatani.** 1993. The *Drosophila* 110-kDa transcription factor TFIID subunit directly interacts with the N-terminal region of the 230-kDa subunit. Proc. Natl. Acad. Sci. USA **90:**5896–5900.
44. **Kokubo, T., D. W. Gong, J. C. Wootton, M. Horikoshi, R. G. Roeder, and Y. Nakatani.** 1994. Molecular cloning of *Drosophila* TFIID subunits. Nature (London) **367:**484–487.
45. **Kokubo, T., D. W. Gong, S. Yamashita, M. Horikoshi, R. G. Roeder, and Y. Nakatani.** 1993. *Drosophila* 230-kD TFIID subunit, a functional homolog of the human cell cycle gene product, negatively regulates DNA binding of the TATA box-binding subunit of TFIID. Genes Dev. **7:**1033–1046.
46. **Kokubo, T., D. W. Gong, S. Yamashita, R. Takada, R. G. Roeder, M. Horikoshi, and Y. Nakatani.** 1993. Molecular cloning, expression, and characterization of the *Drosophila* 85-kilodalton TFIID subunit. Mol. Cell. Biol. **13:**7859–7863.
47. **Kokubo, T., R. Takada, S. Yamashita, D. W. Gong, R. G. Roeder, M. Horikoshi, and Y. Nakatani.** 1993. Identification of TFIID components required for transcriptional activation by upstream stimulatory factor. J. Biol. Chem. **268:**17554–17558.
48. **Kokubo, T., S. Yamashita, M. Horikoshi, R. G. Roeder, and Y. Nakatani.** 1994. Interaction between the N-terminal domain of the 230-kDa subunit and the TATA box-binding subunit of TFIID negatively regulates TATA-box binding. Proc. Natl. Acad. Sci. USA **91:**3520–3524.
49. **Kunkel, T. A., J. D. Roberts, and R. A. Zakour.** 1987. Rapid and efficient site-specific mutagenesis without phenotypic selection. Methods Enzymol. **154:**367–382.
50. **Lavigne, A. C., G. Mengus, M. May, V. Dubrovskaya, L. Tora, P. Chambon, and I. Davidson.** 1996. Multiple interactions between $hTAF_{II}55$ and other TFIID subunits. Requirements for the formation of stable ternary complexes between $hTAF_{II}55$ and the TATA-binding protein. J. Biol. Chem. **271:**19774–19780.
51. **Lu, H., and A. J. Levine.** 1995. Human $TAF_{II}31$ protein is a transcriptional coactivator of the p53 protein. Proc. Natl. Acad. Sci. USA **92:**5154–5158.
52. **Lundblad, J. R., M. Laurance, and R. H. Goodman.** 1996. Fluorescence polarization analysis of protein-DNA and protein-protein interactions. Mol. Endocrinol. **10:**607–612.

53. **Mengus, G., M. May, X. Jacq, A. Staub, L. Tora, P. Chambon, and I. Davidson.** 1995. Cloning and characterization of hTAF$_{II}$18, hTAF$_{II}$20 and hTAF$_{II}$28: three subunits of the human transcription factor TFIID. EMBO J. **14:**1520–1531.
54. **Mizzen, C. A., X.-J. Yang, T. Kokubo, J. E. Brownell, A. J. Bannister, T. Owen-Hughes, J. Workman, L. Wang, S. L. Berger, T. Kouzarides, Y. Nakatani, and C. D. Allis.** 1996. The TAF$_{II}$250 subunit of TFIID has histone acetyltransferase activity. Cell **87:**1261–1270.
55. **Moqtaderi, Z., Y. Bai, D. Poon, P. A. Weil, and K. Struhl.** 1996. TBP-associated factors are not generally required for transcriptional activation in yeast. Nature (London) **383:**188–191.
56. **Mumberg, D., R. Muller, and M. Funk.** 1994. Regulatable promoters of *Saccharomyces cerevisiae*: comparison of transcriptional activity and their use for heterologous expression. Nucleic Acids Res. **22:**5767–5768.
57. **Orphanides, G., T. Lagrange, and D. Reinberg.** 1996. The general transcription factors of RNA polymerase II. Genes Dev. **10:**2657–2683.
58. **Perez, G. M.** Unpublished observations.
59. **Perez, G. M., Y. Bai, P. A. Weil, and J. M. Beechem.** Unpublished observations.
60. **Perez-Howard, G. M., P. A. Weil, and J. M. Beechem.** 1995. Yeast TATA binding protein interaction with DNA: fluorescence determination of oligomeric state, equilibrium binding, on-rate, and dissociation kinetics. Biochemistry **34:**8005–8017.
61. **Poon, D., Y. Bai, A. M. Campbell, S. Bjorklund, Y. J. Kim, S. Zhou, R. D. Kornberg, and P. A. Weil.** 1995. Identification and characterization of a TFIID-like multiprotein complex from *Saccharomyces cerevisiae*. Proc. Natl. Acad. Sci. USA **92:**8224–8228.
62. **Poon, D., S. Schroeder, C. K. Wang, T. Yamamoto, M. Horikoshi, R. G. Roeder, and P. A. Weil.** 1991. The conserved carboxy-terminal domain of *Saccharomyces cerevisiae* TFIID is sufficient to support normal cell growth. Mol. Cell. Biol. **11:**4809–4821.
63. **Poon, D., and P. A. Weil.** 1993. Immunopurification of yeast TATA-binding protein and associated factors. Presence of transcription factor IIIB transcriptional activity. J. Biol. Chem. **268:**15325–15328.
64. **Pugh, B. F., and R. Tjian.** 1990. Mechanism of transcriptional activation by Sp1: evidence for coactivators. Cell **61:**1187–1197.
65. **Reddy, V. B., B. Thimmappaya, R. Dhar, K. N. Subramanian, B. S. Zain, J. Pan, P. K. Ghosh, M. L. Celma, and S. M. Weissman.** 1978. The genome of simian virus 40. Science **200:**494–502.
66. **Reese, J. C., L. Apone, S. S. Walker, L. A. Griffin, and M. R. Green.** 1994. Yeast TAF$_{II}$s in a multisubunit complex required for activated transcription. Nature (London) **371:**523–527.
67. **Roeder, R. G.** 1991. The complexities of eukaryotic transcription initiation: regulation of preinitiation complex assembly. Trends Biochem. Sci. **16:**402–408.
68. **Rosenberg, A. H., B. N. Lade, D. S. Chui, S. W. Lin, J. J. Dunn, and F. W. Studier.** 1987. Vectors for selective expression of cloned DNAs by T7 RNA polymerase. Gene **56:**125–135.
69. **Rothstein, R. J.** 1983. One-step gene disruption in yeast. Methods Enzymol. **101:**202–211.
70. **Ruppert, S., and R. Tjian.** 1995. Human TAF$_{II}$250 interacts with RAP74: implications for RNA polymerase II initiation. Genes Dev. **9:**2747–2755.
71. **Ruppert, S., E. H. Wang, and R. Tjian.** 1993. Cloning and expression of human TAF$_{II}$250: a TBP-associated factor implicated in cell-cycle regulation. Nature (London) **362:**175–179.
72. **Sauer, F., S. K. Hansen, and R. Tjian.** 1995. Multiple TAF$_{II}$s directing synergistic activation of transcription. Science **270:**1783–1788.
73. **Sekiguchi, T., T. Miyata, and T. Nishimoto.** 1988. Molecular cloning of the cDNA of human X chromosomal gene (*CCG1*) which complements the temperature-sensitive G1 mutants, tsBN462 and ts13, of the BHK cell line. EMBO J. **7:**1683–1687.
74. **Sekiguchi, T., Y. Nohiro, Y. Nakamura, N. Hisamoto, and T. Nishimoto.** 1991. The human *CCG1* gene, essential for progression of the G$_1$ phase, encodes a 210-kilodalton nuclear DNA-binding protein. Mol. Cell. Biol. **11:**3317–3325.
75. **Shao, Z., S. Ruppert, and P. D. Robbins.** 1995. The retinoblastoma-susceptibility gene product binds directly to the human TATA-binding protein-associated factor TAF$_{II}$250. Proc. Natl. Acad. Sci. USA **92:**3115–3119.
76. **Sikorski, R. S., and P. Hieter.** 1989. A system of shuttle vectors and yeast host strains designed for efficient manipulation of DNA in *Saccharomyces cerevisiae*. Genetics **122:**19–27.
77. **Studier, F. W., A. H. Rosenberg, J. J. Dunn, and J. W. Dubendorff.** 1990. Use of T7 RNA polymerase to direct expression of cloned genes. Methods Enzymol. **185:**60–89.
78. **Sypes, M. A., and D. S. Gilmour.** 1994. Protein/DNA crosslinking of a TFIID complex reveals novel interactions downstream of the transcription start. Nucleic Acids Res. **22:**807–814.
79. **Takada, R., Y. Nakatani, A. Hoffmann, T. Kokubo, S. Hasegawa, R. G. Roeder, and M. Horikoshi.** 1992. Identification of human TFIID components and direct interaction between a 250-kDa polypeptide and the TATA box-binding protein (TFIID tau). Proc. Natl. Acad. Sci. USA **89:**11809–11813.
80. **Tanese, N., D. Saluja, M. F. Vassallo, J.-L. Chen, and A. Admon.** 1996. Molecular cloning and analysis of two subunits of the human TFIID complex: hTAF$_{II}$130 and hTAF$_{II}$100. Proc. Natl. Acad. Sci. USA **93:**13611–13616.
81. **Thut, C. J., J. L. Chen, R. Klemm, and R. Tjian.** 1995. p53 transcriptional activation mediated by coactivators TAF$_{II}$40 and TAF$_{II}$60. Science **267:**100–104.
82. **Verrijzer, C. P., J. L. Chen, K. Yokomori, and R. Tjian.** 1995. Binding of TAFs to core elements directs promoter selectivity by RNA polymerase II. Cell **81:**1115–1125.
83. **Verrijzer, C. P., K. Yokomori, J. L. Chen, and R. Tjian.** 1994. *Drosophila* TAF$_{II}$150: similarity to yeast gene *TSM-1* and specific binding to core promoter DNA. Science **264:**933–941.
84. **Walker, S. S., J. C. Reese, L. M. Apone, and M. R. Green.** 1996. Transcription activation in cells lacking TAF$_{II}$s. Nature (London) **383:**185–188.
85. **Wang, E. H., and R. Tjian.** 1994. Promoter-selective transcriptional defect in cell cycle mutant ts13 rescued by hTAF$_{II}$250. Science **263:**811–814.
86. **Weinzierl, R. O., B. D. Dynlacht, and R. Tjian.** 1993. Largest subunit of *Drosophila* transcription factor IID directs assembly of a complex containing TBP and a coactivator. Nature (London) **362:**511–517.
87. **Weinzierl, R. O., S. Ruppert, B. D. Dynlacht, N. Tanese, and R. Tjian.** 1993. Cloning and expression of *Drosophila* TAF$_{II}$60 and human TAF$_{II}$70 reveal conserved interactions with other subunits of TFIID. EMBO J. **12:**5303–5309.
88. **Wilson, I. A., H. L. Niman, R. A. Houghten, A. R. Cherenson, M. L. Connolly, and R. A. Lerner.** 1984. The structure of an antigenic determinant in a protein. Cell **37:**767–778.
89. **Yokomori, K., J. L. Chen, A. Admon, S. Zhou, and R. Tjian.** 1993. Molecular cloning and characterization of dTAF$_{II}$30 alpha and dTAF$_{II}$30 beta: two small subunits of *Drosophila* TFIID. Genes Dev. **7:**2587–2597.
90. **Yokomori, K., M. P. Zeidler, J. L. Chen, C. P. Verrijzer, M. Mlodzik, and R. Tjian.** 1994. *Drosophila* TFIIA directs cooperative DNA binding with TBP and mediates transcriptional activation. Genes Dev. **8:**2313–2323.
91. **Zhou, Q., T. G. Boyer, and A. J. Berk.** 1993. Factors (TAFs) required for activated transcription interact with TATA box-binding protein conserved core domain. Genes Dev. **7:**180–187.
92. **Zhou, Q., P. M. Lieberman, T. G. Boyer, and A. J. Berk.** 1992. Holo-TFIID supports transcriptional stimulation by diverse activators and from a TATA-less promoter. Genes Dev. **6:**1964–1974.